

LHC phenomenology of the type II seesaw mechanism: Observability of neutral scalars in the nondegenerate case

Zhi-Long Han ^{1,*} Ran Ding ^{2,†} and Yi Liao ^{3,2,1‡}

¹ *School of Physics, Nankai University, Tianjin 300071, China*

² *Center for High Energy Physics, Peking University, Beijing 100871, China*

³ *State Key Laboratory of Theoretical Physics, Institute of Theoretical Physics,
Chinese Academy of Sciences, Beijing 100190, China*

(Dated: September 8, 2015)

This is a sequel to our previous work on LHC phenomenology of the type II seesaw model in the nondegenerate case. In this work, we further study the pair and associated production of the neutral scalars H^0/A^0 . We restrict ourselves to the so-called negative scenario characterized by the mass order $M_{H^{\pm\pm}} > M_{H^\pm} > M_{H^0/A^0}$, in which the H^0/A^0 production receives significant enhancement from cascade decays of the charged scalars $H^{\pm\pm}$, H^\pm . We consider three important signal channels— $b\bar{b}\gamma\gamma$, $b\bar{b}\tau^+\tau^-$, $b\bar{b}\ell^+\ell^- \cancel{E}_T$ —and perform detailed simulations. We find that at the 14 TeV LHC with an integrated luminosity of 3000 fb^{-1} , a 5σ mass reach of 151, 150, and 180 GeV, respectively, is possible in the three channels from the pure Drell-Yan $H^0 A^0$ production, while the cascade-decay-enhanced H^0/A^0 production can push the mass limit further to 164, 177, and 200 GeV. The neutral scalars in the negative scenario are thus accessible at LHC run II.

* hanzhilong@mail.nankai.edu.cn

† dingran@mail.nankai.edu.cn

‡ liaoy@nankai.edu.cn

I. INTRODUCTION

In a previous paper [1], we presented a comprehensive analysis on the LHC signatures of the type II seesaw model of neutrino masses in the nondegenerate case of the triplet scalars. In this companion paper, another important signature—the pair and associated production of the neutral scalars—is explored in great detail. This is correlated to the pair production of the standard model (SM) Higgs boson, h , which has attracted lots of theoretical and experimental interest [2, 3] since its discovery [4, 5], because the pair production can be used to gain information on the electroweak symmetry breaking sector [6]. Since any new ingredients in the scalar sector can potentially alter the production and decay properties of the Higgs boson, a thorough examination of the properties offers a diagnostic tool to physics effects beyond the SM. The Higgs boson pair production has been well studied for collider phenomenology in the framework of the SM and beyond [6–22], and extensively studied in various new physics models [23–47], as well as in the effective field theory approach of anomalous couplings [48–51] and effective operators [52–56].

The pair production of the SM Higgs boson proceeds dominantly through the gluon fusion process [6, 8], and has a cross section at the 14 TeV LHC (LHC14) of about 18 fb at leading order [6].¹ It can be utilized to measure the Higgs trilinear coupling. A series of studies have surveyed its observability in the $b\bar{b}\gamma\gamma$, $b\bar{b}\tau^+\tau^-$, $b\bar{b}W^+W^-$, $b\bar{b}b\bar{b}$, and WW^*WW^* signal channels [11–13, 21, 22, 36, 57]. For the theoretical and experimental status of the Higgs trilinear coupling and pair production at the LHC, see Refs. [57, 58]. In summary, at the 14 TeV LHC with an integrated luminosity of 3000 fb⁻¹ (LHC14@3000), the trilinear coupling could be measured at an accuracy of $\sim 40\%$ [18], and thus leaves potential space for new physics.

As we pointed out in Ref. [1], in the negative scenario of the type II seesaw model where the doubly charged scalars $H^{\pm\pm}$ are the heaviest and the neutral ones H^0/A^0 the lightest, i.e., $M_{H^{\pm\pm}} > M_{H^\pm} > M_{H^0/A^0}$, the associated H^0A^0 production gives the same signals as the SM Higgs pair production while enjoying a larger cross section. The leading production channel is the Drell-Yan process $pp \rightarrow Z^* \rightarrow H^0A^0$, with a typical cross section 20-500 fb in the mass region 130-300 GeV. Additionally, there exists a sizable enhancement from the cascade decays of the heavier charged scalars, which also gives some indirect evidence for these particles. The purpose of this paper is to examine the importance of the H^0A^0 production with an emphasis on the contribution from cascade decays and to explore their observability.

The paper is organized as follows. In Sec. II, we summarize the relevant part of the type II seesaw and explore the decay properties of H^0 , A^0 in the negative scenario. Sections III and IV contain our systematical analysis of the impact of cascade decays on the H^0/A^0 production in the three signal channels, $b\bar{b}\gamma\gamma$, $b\bar{b}\tau^+\tau^-$, and $b\bar{b}\ell^+\ell^- \cancel{E}_T$. We discuss the observability of the signals and estimate the required integrated

¹ This number is modified to 33 fb at next-to-leading order [7] and to 40 fb at next-to-next-to-leading order [16].

luminosity for a certain mass reach and significance. Discussions and conclusions are presented in Sec. V. In most cases, we will follow the notations and conventions in Ref. [1].

II. DECAY PROPERTIES OF NEUTRAL SCALARS IN THE NEGATIVE SCENARIO

The type II seesaw and its various experimental constraints have been reviewed in our previous work [1]. Here we recall the most relevant content that is necessary for our study of the decay properties of the scalars in this section and of their detection at the LHC in later sections.

The type II seesaw model introduces an extra scalar triplet Δ of hypercharge two [59] on top of the SM Higgs doublet Φ of hypercharge unity. Writing Δ in matrix form, the most general scalar potential is

$$V(\Phi, \Delta) = m^2 \Phi^\dagger \Phi + M^2 \text{Tr}(\Delta^\dagger \Delta) + \lambda_1 (\Phi^\dagger \Phi)^2 + \lambda_2 \left(\text{Tr}(\Delta^\dagger \Delta) \right)^2 + \lambda_3 \text{Tr}(\Delta^\dagger \Delta)^2 + \lambda_4 (\Phi^\dagger \Phi) \text{Tr}(\Delta^\dagger \Delta) + \lambda_5 \Phi^\dagger \Delta \Delta^\dagger \Phi + \left(\mu \Phi^T i \tau^2 \Delta^\dagger \Phi + \text{H.c.} \right). \quad (1)$$

As in the SM, $m^2 < 0$ is assumed to trigger spontaneous symmetry breaking, while $M^2 > 0$ sets the mass scale of the new scalars. The vacuum expectation value (vev) v of Φ then induces via the μ term a vev v_Δ for Δ . The components of equal charge (and also of identical CP in the case of neutral components) in Δ and Φ then mix into physical scalars H^\pm ; A^0 ; H^0 , h and would-be Goldstone bosons $G^{\pm,0}$, with the mixing angles specified by (see, for instance, Refs. [60, 61])

$$\tan \theta_+ = \frac{\sqrt{2}v_\Delta}{v}, \quad \tan \alpha = \frac{2v_\Delta}{v}, \quad \tan 2\theta_0 = \frac{2v_\Delta}{v} \frac{v^2(\lambda_4 + \lambda_5) - 2M_\Delta^2}{2v^2\lambda_1 - M_\Delta^2 - v_\Delta^2(\lambda_2 + \lambda_3)}, \quad (2)$$

where an auxiliary parameter is introduced for convenience,

$$M_\Delta^2 = \frac{v^2 \mu}{\sqrt{2}v_\Delta}. \quad (3)$$

To a good approximation, the SM-like Higgs boson h has the mass $M_h \approx \sqrt{2\lambda_1}v$, the new neutral scalars H^0 , A^0 have an equal mass $M_{H^0} \approx M_{A^0} \approx M_\Delta$, and the new scalars of various charges are equidistant in squared masses:

$$M_{H^{\pm\pm}}^2 - M_{H^\pm}^2 \approx M_{H^\pm}^2 - M_{H^0/A^0}^2 \approx -\frac{1}{4}\lambda_5 v^2. \quad (4)$$

There are thus two scenarios of spectra, positive or negative, according to the sign of λ_5 . For convenience, we define $\Delta M \equiv M_{H^\pm} - M_{H^0/A^0}$.

In the rest of this section, we discuss the decay properties of the new scalars in the negative scenario with an emphasis on H^0 and A^0 . The explicit expressions for the relevant decay widths can be found in Refs. [62–64]. It has been shown that H^0/A^0 decays dominantly into neutrinos for $v_\Delta < 10^{-4}$ GeV [65],

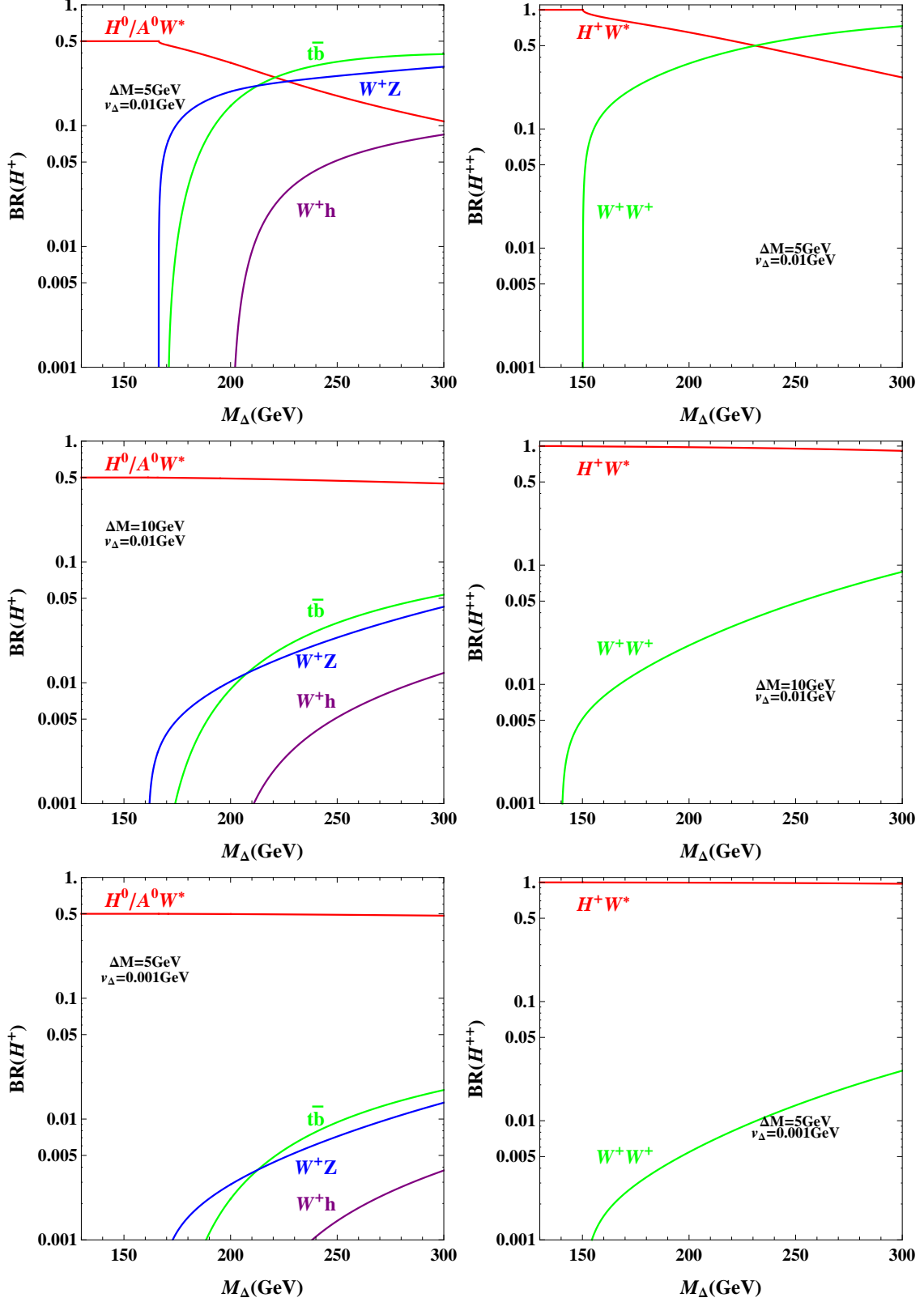


FIG. 1. Branching ratios of H^\pm and $H^{\pm\pm}$ versus M_Δ at some benchmark points of ΔM and v_Δ : $(\Delta M, v_\Delta) = (5, 0.01), (10, 0.01), (5, 0.001) \text{ GeV}$, from the upper to the lower panels.

resulting in totally invisible final states. We will restrict ourselves to $v_\Delta \gg 10^{-4}$ GeV in this work, where H^0/A^0 dominantly decays into visible particles. Before we detail their decay properties, we give a brief account of the cascade decays of the charged scalars. The branching ratios of the cascade decays are controlled by the three parameters, v_Δ , ΔM , and M_Δ . The cascade decays dominate in the moderate region of v_Δ and for ΔM not too small, where a minimum value of $\Delta M \sim 2$ GeV appears around $v_\Delta \sim 10^{-4}$ GeV [1, 62, 65, 66]. In Fig. 1, the branching ratios of H^\pm and $H^{\pm\pm}$ are shown as a function of M_Δ at some benchmark points of v_Δ and ΔM . Basically speaking, in the mass region $M_\Delta = 130$ -300 GeV, the cascade decays are dominant for a relatively large mass splitting ΔM (as shown in the middle panel of Fig. 1) or a relatively small v_Δ (in the lower panel).

A. H^0 decays

At tree level, H^0 can decay to $f\bar{f}$ ($f = q, l$), $\nu\nu$, W^+W^- , ZZ , and hh . It can also decay to gg , $\gamma\gamma$, and $Z\gamma$ through radiative effects. Similarly, $A^0 \rightarrow f\bar{f}$, $\nu\nu$, Zh at tree level, and it has the same decay modes as H^0 at the loop level. Since we have chosen $v_\Delta \gg 10^{-4}$ GeV, the neutrino mode can be safely neglected for both H^0 and A^0 . Previous work usually concentrated on the decoupling region where the neutral scalars H^0/A^0 are much heavier than the light CP -even Higgs h and the scalar self-couplings λ_i are taken to be zero for simplicity [65]. In this case, the mixing angle $\theta_0 \approx \alpha$, and the $H^0W^+W^-$ coupling [being proportional to $\sin(\alpha - \theta_0)$] tends to vanish. As a consequence, the W -pair mode is absent and the dominant channels are $H^0 \rightarrow hh, ZZ$ for a heavy H^0 . In contrast, we take into account the effect of scalar self-interactions and focus on the nondecoupling regime, i.e., H^0/A^0 are not much heavier than h .

For illustration, we choose the benchmark values $v_\Delta = 10^{-3}$ GeV, $\Delta M = 5$ GeV; then, λ_5 is determined by Eq. (4) upon specifying M_Δ .² To investigate the effect of the scalar self-interactions, we note the following features in the decays of H^0 . 1) The decay widths of $H^0 \rightarrow f\bar{f}, gg$ differ from those of h only by a factor of $\sin^2 \theta_0$, which leads to similar behavior for H^0 and h . 2) The only free parameter for the mixing between H^0 and h is λ_4 , because [as shown in Eq. (2)] the impact of $\lambda_{2,3}$ is suppressed by a small v_Δ and a relatively large mass difference between M_Δ and M_h while λ_1 is fixed by M_h . 3) λ_4 enters the $H^0W^+W^-$ and H^0ZZ couplings and thus affects the decays $H^0 \rightarrow W^+W^-, ZZ$. 4) The H^0hh coupling simplifies for $v_\Delta \ll v$ such that the only free parameter in the decay $H^0 \rightarrow hh$ is again λ_4 . As a consequence of these features, we shall choose λ_4 as a free parameter and vary it in the range $[-1.0, 1.0]$, and fix the couplings $\lambda_2 = \lambda_3 = 0.1$ which are involved in loop-induced decays.

We first examine the branching ratios of $H^0 \rightarrow f\bar{f}$. $\text{BR}(H^0 \rightarrow b\bar{b})$ and $\text{BR}(H^0 \rightarrow t\bar{t})$ are plotted in

² As pointed out in Ref. [62], varying v_Δ in the range 10^{-3} -1 GeV would not change the branching ratios significantly.

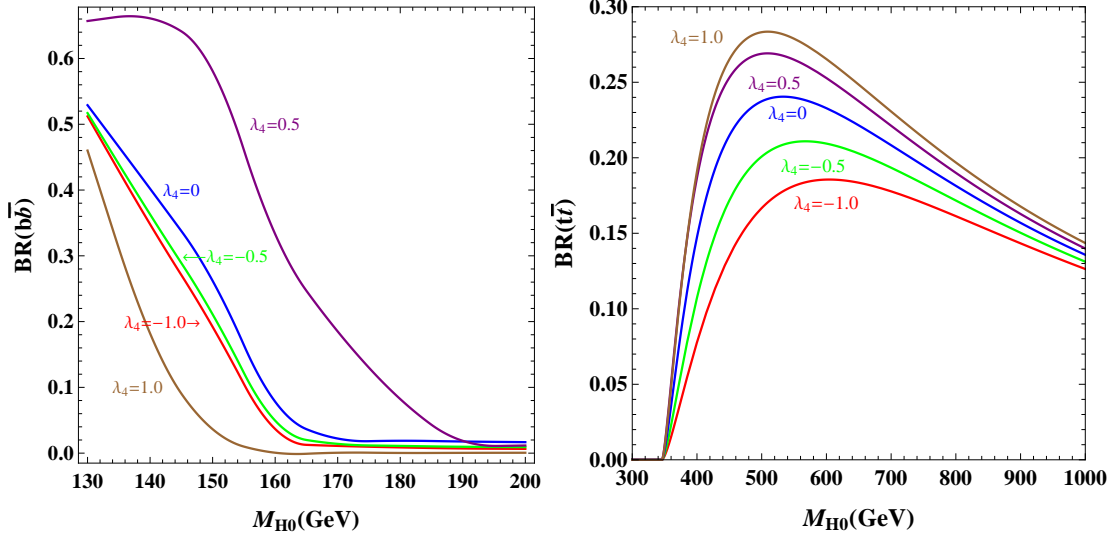


FIG. 2. Branching ratios of $H^0 \rightarrow b\bar{b}$ and $H^0 \rightarrow t\bar{t}$ as a function of M_{H^0} for various values of λ_4 .

Fig. 2 for different mass regions of H^0 .³ It is clear that the variation of $BR(H^0 \rightarrow b\bar{b})$ is more dramatic for $\lambda_4 > 0$. The maximum of $BR(H^0 \rightarrow b\bar{b})$ appears at $\lambda_4 \approx 0.5$. Obviously, $BR(H^0 \rightarrow b\bar{b})$ is a nonmonotonic function of λ_4 , while $BR(H^0 \rightarrow t\bar{t})$ monotonically increases with λ_4 . As will be discussed later, this different behavior in the two mass regions is due mainly to a zero in the $H^0 ZZ$ coupling.

Now we study the bosonic decays $H^0 \rightarrow W^+W^-$, ZZ , hh . In the left panel of Fig. 3, we present the branching ratios of $H^0 \rightarrow W^+W^-$, ZZ in the mass region 130-300 GeV. For most values of λ_4 , $BR(H^0 \rightarrow W^+W^-)$ increases with M_{H^0} when $M_{H^0} < 2M_W$, and varying λ_4 for $\lambda_4 > 0$ changes it considerably. λ_4 has a strong impact on $BR(H^0 \rightarrow W^+W^-)$ in the mass region $2M_Z < M_{H^0} < 2M_h$ where the decay channel dominates overwhelmingly for $\lambda_4 < 0$ but becomes negligible for λ_4 approaching about 0.5. However, once the $H^0 \rightarrow hh$ channel is opened, $H^0 \rightarrow W^+W^-$ is suppressed significantly independent of λ_4 . The decay $H^0 \rightarrow ZZ$ cannot dominate when $M_{H^0} < 2M_W$. In the mass region $2M_Z < M_{H^0} < 2M_h$, it is complementary with the W^+W^- channel, so their behavior is just opposite. More interestingly, there is a zero point for the $H^0 ZZ$ coupling, which is proportional to $(v \sin \theta_0 - 4v_\Delta \cos \theta_0)$. According to Eq. (2), one obtains the corresponding M_Δ at the zero:

$$M_\Delta^0(ZZ) = \sqrt{2M_h^2 - \frac{1}{2}(\lambda_4 + \lambda_5)v^2}. \quad (5)$$

Note that the above relation only holds for $\lambda_4 + \lambda_5 < 2M_h^2/v^2 \approx 0.5$, since we are working in the scenario where $M_\Delta > M_h$. The existence of the zero coupling explains the presence of the nodes in $BR(H^0 \rightarrow ZZ)$ for $\lambda_4 \leq 0$.

³ The influence of λ_4 for light fermions b, c, τ, μ and gluons is similar, so we only present $BR(H^0 \rightarrow b\bar{b})$ in Fig. 2.

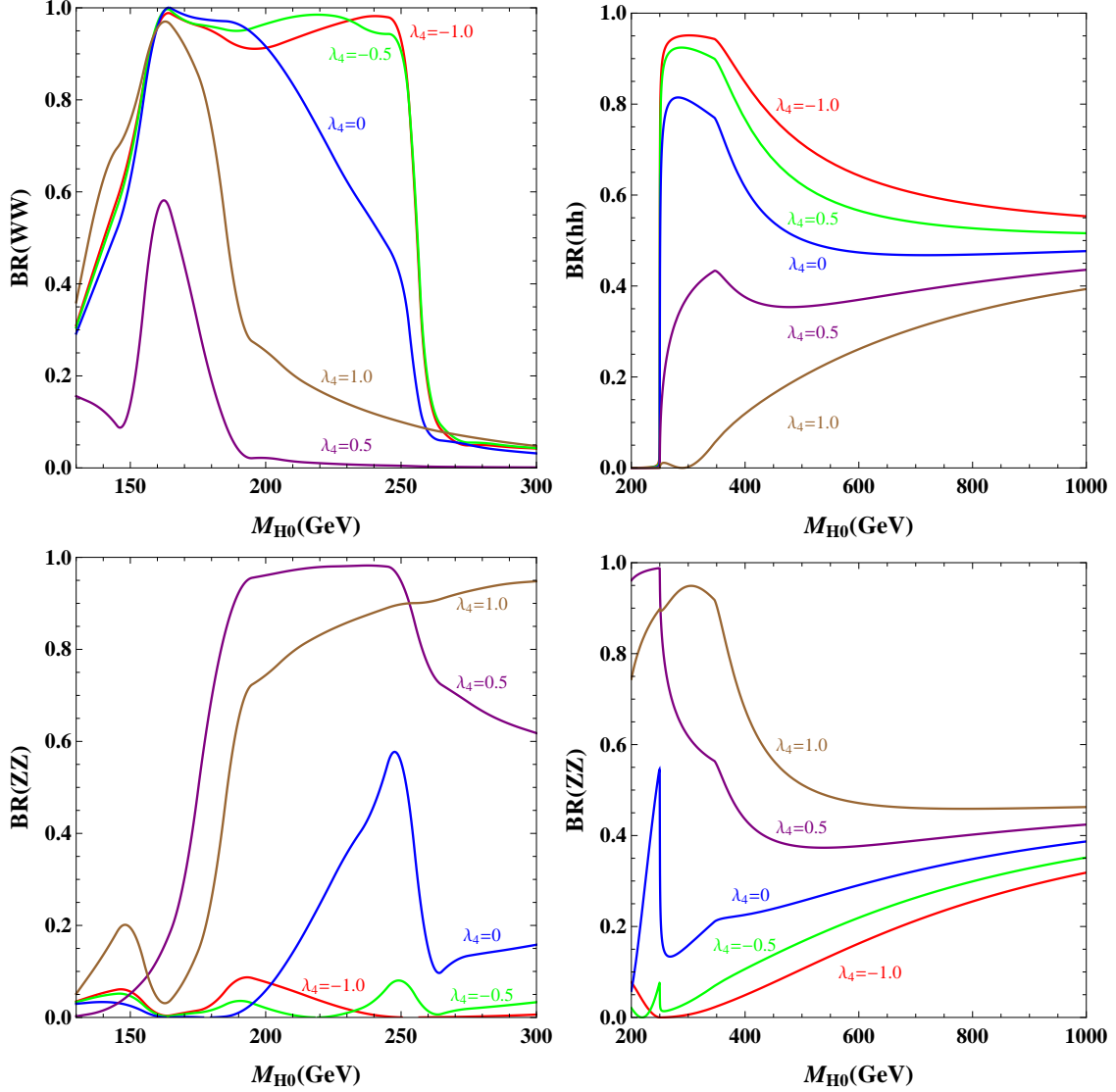


FIG. 3. Left: Branching ratios of $H^0 \rightarrow W^+W^-$, ZZ as a function of M_{H^0} in the mass region 130-300 GeV. Right: Branching ratios of $H^0 \rightarrow hh$, ZZ as a function of M_{H^0} in the mass region 200-1000 GeV.

In the right panel of Fig. 3, $\text{BR}(H^0 \rightarrow hh, ZZ)$ are shown in the mass region 200-1000 GeV. When $M_{H^0} > 2M_h$, the dependence on λ_4 is simple: a larger λ_4 corresponds to a smaller $\text{BR}(H^0 \rightarrow hh)$ and a larger $\text{BR}(H^0 \rightarrow ZZ)$. It is clear that λ_4 has a more significant impact in the mass region 200 ~ 350 GeV, and varying λ_4 could change $\text{BR}(H^0 \rightarrow ZZ)$ from 0 to 0.9. Once M_{H^0} exceeds $2M_t$, the evolution of $\text{BR}(H^0 \rightarrow hh, ZZ)$ becomes smooth with the increase of M_{H^0} . There also exists a zero point for the $H^0 hh$ coupling, which can be obtained as for the ZZ channel:

$$M_{\Delta}^0(hh) = \sqrt{2(\lambda_4 + \lambda_5)v^2 - 2M_h^2}, \quad (6)$$

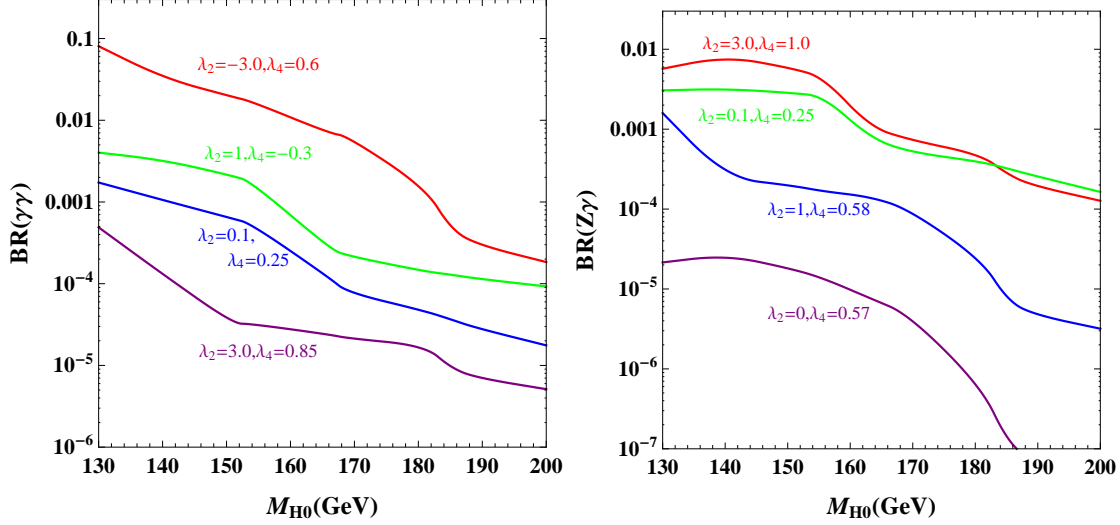


FIG. 4. Branching ratios of $H^0 \rightarrow \gamma\gamma$, $Z\gamma$ as a function of M_{H^0} for various sets of $\lambda_{2,4}$ values.

which is valid for $\lambda_4 + \lambda_5 > 3M_h^2/2v^2 \approx 0.375$.

Finally, we investigate the loop-induced decays, $H^0 \rightarrow \gamma\gamma$, $Z\gamma$. In addition to the usual contributions from the top quark and W boson, the new charged scalars H^\pm and $H^{\pm\pm}$ also contribute to the decays. These new terms involve the $H^0 H^+ H^-$ and $H^0 H^{++} H^{--}$ couplings, which are proportional to

$$\begin{aligned} H^0 H^+ H^- &: [(2\lambda_2 + 2\lambda_3 - \lambda_5) \sin \alpha \cos \theta_0 - (2\lambda_4 + \lambda_5) \cos \alpha \sin \theta_0], \\ H^0 H^{++} H^{--} &: (\lambda_2 \sin \alpha \cos \theta_0 - \lambda_4 \cos \alpha \sin \theta_0). \end{aligned} \quad (7)$$

One therefore has to consider the scalar self-couplings $\lambda_{2,3}$. For simplicity, we set $\lambda_2 = \lambda_3$ and vary them from -3.0 to 3.0 . In Fig. 4, we display $\text{BR}(H^0 \rightarrow \gamma\gamma)$ and $\text{BR}(H^0 \rightarrow Z\gamma)$ versus M_{H^0} for some typical sets of $\lambda_{2,4}$ values. The evolution of both branching ratios crosses 3 orders of magnitude in this parameter region. The resulting enhancement compared with $h \rightarrow \gamma\gamma$ in the SM looks significant: the maximal enhancement can be achieved at the level of 9% for the $H^0 \rightarrow \gamma\gamma$ channel at $M_{H^0} = 130$ GeV, and of 0.7% for the $H^0 \rightarrow Z\gamma$ channel at $M_{H^0} \approx 140$ GeV.

B. A^0 decays

Similar to H^0 , the decay widths of $A^0 \rightarrow f\bar{f}$, gg differ from those of h by a factor of $\sin^2 \alpha$ with α being given in Eq. (2). Moreover, the only vertex which involves λ_i is the $A^0 Zh$ coupling proportional to $(\cos \theta_0 \sin \alpha - 2 \sin \theta_0 \cos \alpha)$. As a consequence, one can only choose λ_4 as a free parameter to illustrate the influence of scalar interactions. In this section, we also vary λ_4 from -1.0 to 1.0 and take the same benchmark values for v_Δ and ΔM as for the H^0 decays.

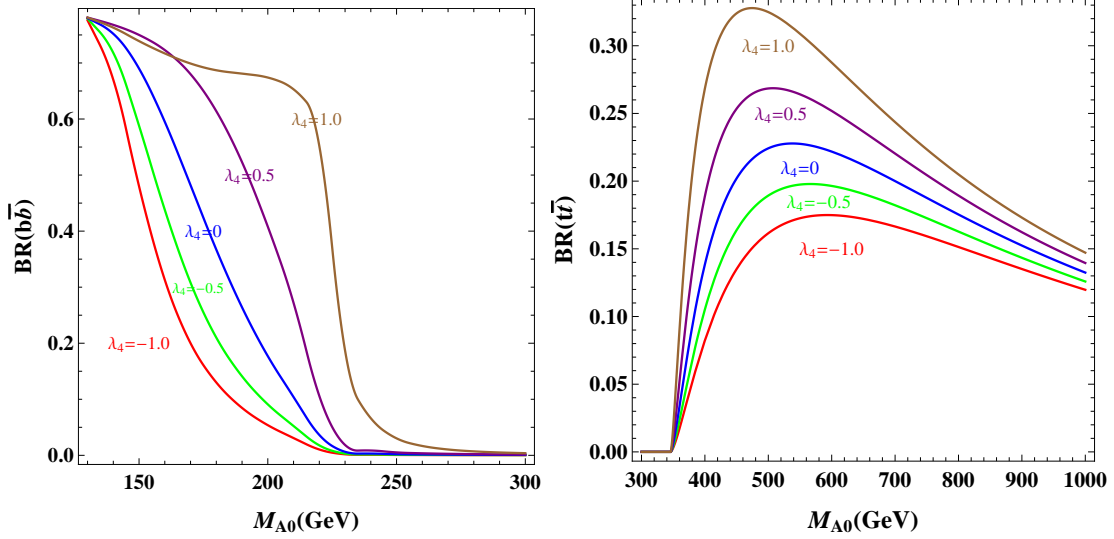


FIG. 5. Branching ratios of $A^0 \rightarrow b\bar{b}$, $t\bar{t}$ as a function of M_{A^0} for various values of λ_4 .

In the left panel of Fig. 5, we present $\text{BR}(A^0 \rightarrow b\bar{b})$ as a function of M_{A^0} .⁴ For a fixed value of λ_4 , $\text{BR}(A^0 \rightarrow b\bar{b})$ decreases as M_{A^0} increases. The dependence of $\text{BR}(A^0 \rightarrow b\bar{b})$ on λ_4 is simple: The larger λ_4 is, the larger $\text{BR}(A^0 \rightarrow b\bar{b})$ is. And $\text{BR}(A^0 \rightarrow b\bar{b})$ can be dominant with $\lambda_4 = 1.0$ as long as $A^0 \rightarrow Zh$ is not fully opened. The right panel of Fig. 5 shows $\text{BR}(A^0 \rightarrow t\bar{t})$, which is very similar to $\text{BR}(H^0 \rightarrow t\bar{t})$.

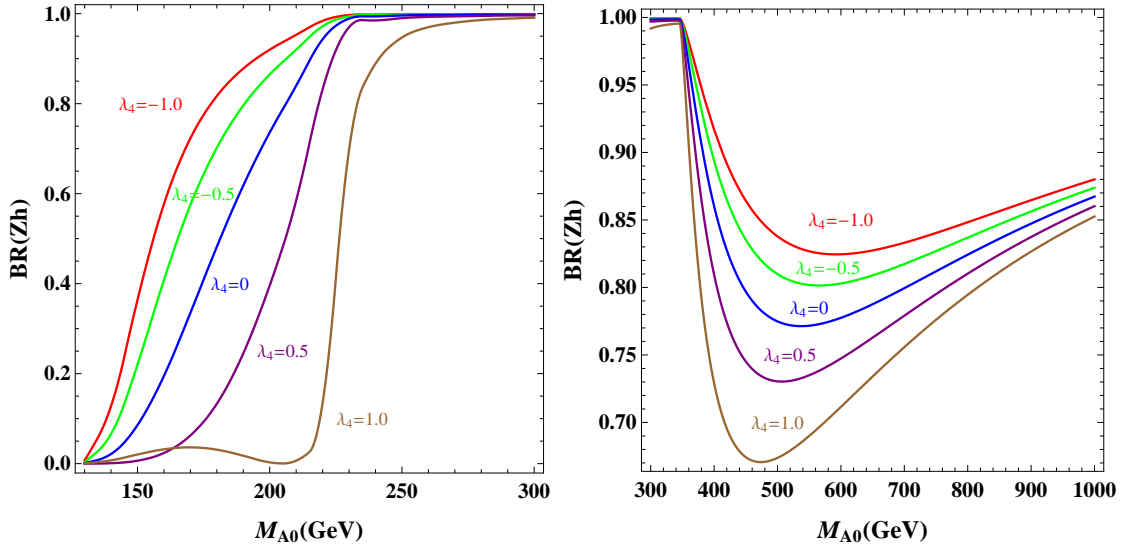


FIG. 6. Branching ratios of $A^0 \rightarrow Zh$ as a function of M_{A^0} for various values of λ_4 .

We then study the most important decay $A^0 \rightarrow Zh$. In Fig. 6, we present $\text{BR}(A^0 \rightarrow Zh)$ as a function

⁴ As before, the influence of λ_4 on the $A^0 \rightarrow f\bar{f}$, gg channels is similar to the $b\bar{b}$ mode.

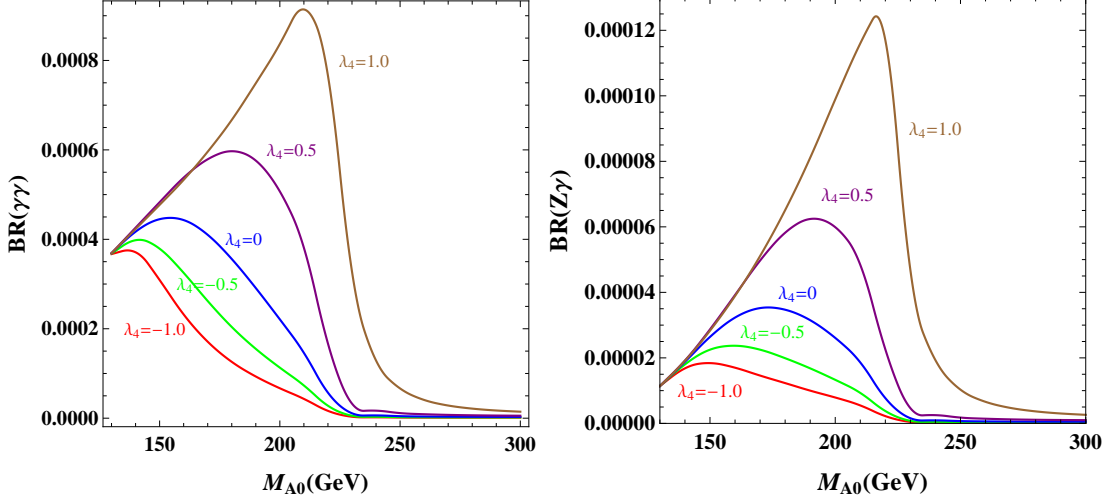


FIG. 7. Branching ratios of $A^0 \rightarrow \gamma\gamma$ and $A^0 \rightarrow Z\gamma$ as a function of M_{A^0} for various values of λ_4 .

of M_{A^0} in the low-mass region (130-300 GeV) and high-mass region (300-1000 GeV), respectively. The evolution of $\text{BR}(A^0 \rightarrow Zh)$ with M_{A^0} and λ_4 is just opposite to that of $A^0 \rightarrow b\bar{b}$ ($t\bar{t}$) in the low- (high-) mass region. The variation of $\text{BR}(A^0 \rightarrow Zh)$ with λ_4 is dramatic below the Zh threshold. In particular, near the Zh threshold $\text{BR}(A^0 \rightarrow Zh) \sim 1.0$ for $\lambda_4 = -1.0$, while $\text{BR}(A^0 \rightarrow Zh)$ tends to vanish for $\lambda_4 = 1.0$, which corresponds to the zero point of the $A^0 Zh$ coupling:

$$M_{\Delta}^0(Zh) = \sqrt{(\lambda_4 + \lambda_5)v^2 - M_h^2}, \quad (8)$$

with $\lambda_4 + \lambda_5 > 2M_h^2/v^2 \approx 0.5$. $\text{BR}(A^0 \rightarrow Zh)$ is totally dominant in the mass region between the Zh and $t\bar{t}$ thresholds, and becomes comparable to $\text{BR}(A^0 \rightarrow t\bar{t})$ when $M_{A^0} > 2M_t$.

At last, we study the one-loop-induced decays, $A^0 \rightarrow \gamma\gamma$, $Z\gamma$. These two channels can only be induced by the top quark in the loop since the $A^0 W^+ W^-$, $A^0 H^+ H^-$, and $A^0 H^{++} H^{--}$ couplings are absent in the CP -conserving case. In Fig. 7, both $\text{BR}(A^0 \rightarrow \gamma\gamma)$ and $\text{BR}(A^0 \rightarrow Z\gamma)$ are displayed. For M_{A^0} below the Zh threshold, the variation in λ_4 of $\text{BR}(A^0 \rightarrow \gamma\gamma)$ increases as M_{A^0} increases. $\text{BR}(A^0 \rightarrow \gamma\gamma)$ could reach 9×10^{-4} for $M_{A^0} \approx 210$ GeV and $\lambda_4 = 1.0$, which is much smaller than the maximum of $\text{BR}(H^0 \rightarrow \gamma\gamma)$. The variation in λ_4 of $\text{BR}(A^0 \rightarrow Z\gamma)$ is slightly steeper, with a maximum of 1.2×10^{-4} at $M_{A^0} \approx 215$ GeV and $\lambda_4 = 1.0$.

In the above, we have discussed the decay channels of H^0 and A^0 separately. We have shown that the scalar self-interactions have a large impact on their branching ratios. In Sec. IV, we will explore their LHC signatures. For this purpose, we choose the following benchmark values:

$$v_{\Delta} = 0.001 \text{ GeV}, \Delta M = 5 \text{ GeV}, \lambda_2 = \lambda_3 = 0.1, \lambda_4 = 0.25. \quad (9)$$

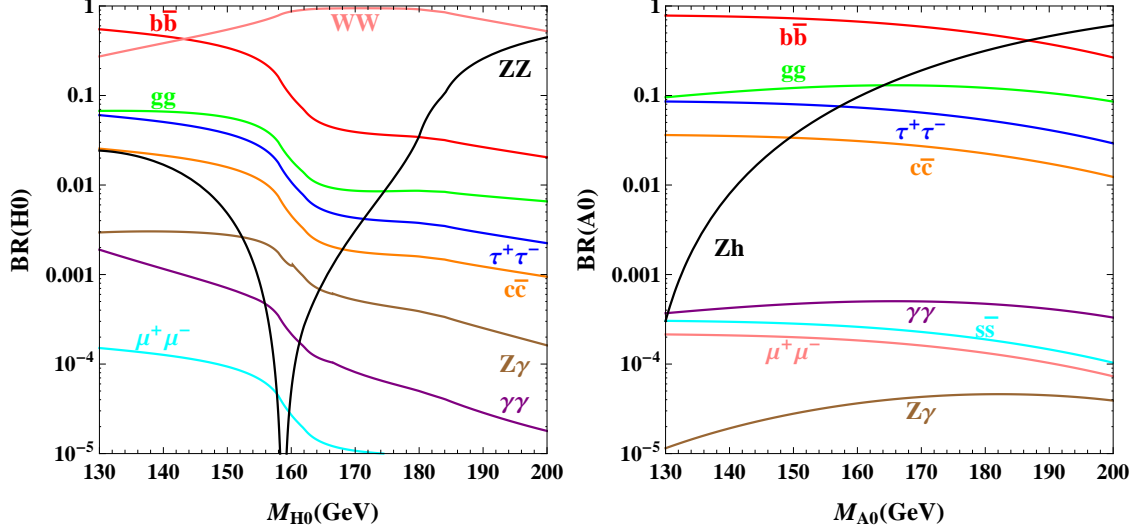


FIG. 8. Branching ratios of H^0/A^0 as a function of M_{H^0/A^0} at the benchmark point in Eq. (9).

The reason that we set relatively small values of v_Δ and ΔM is to obtain large cascade decays of charged scalars as well as a large enhancement of neutral scalar production. In Fig. 8, we display all relevant branching ratios versus M_{H^0/A^0} for this benchmark model, which is to be simulated in Sec. IV for the LHC in the $b\bar{b}\gamma\gamma$, $b\bar{b}\tau^+\tau^-$, and $b\bar{b}W^+W^-$ signal channels.

III. PRODUCTION OF NEUTRAL HIGGS FROM CASCADE DECAYS

We pointed out in Ref. [1] the importance of the associated $H^0 A^0$ production in the nondegenerate case. To estimate the number of signal events, we simulated the signal channel $b\bar{b}\tau^+\tau^-$ at $M_{H^0/A^0} = 130$ GeV. We found that, with a much higher production cross section than the SM Higgs pair (hh) production, a 2.9σ excess in that signal channel is achievable for LHC14@300. In the present work, we are interested in the observability of the associated $H^0 A^0$ production in the nondecoupling mass regime (130-200 GeV). In Fig. 9 we first show the production cross sections for a pair of various scalars at LHC14 versus M_Δ with a degenerate spectrum. As before, we incorporate the next-to-leading-order (NLO) QCD effects by multiplying a K -factor of 1.3 in all $q\bar{q}$ production channels [7]. The hh production through gluon-gluon fusion at NLO (33 fb) is also indicated (black dashed line) for comparison. One can see that the cross section for $H^0 A^0$ is about 20-500 fb in the mass region 130-300 GeV, which is much larger than the hh production for most of the mass region and thus leads to great discovery potential.

In general, the new scalars are nondegenerate for a nonzero λ_5 . In the positive scenario where $H^{\pm\pm}$ are the lightest, the cascade decays of H^\pm and H^0/A^0 can strengthen the observability of $H^{\pm\pm}$ [67, 68].

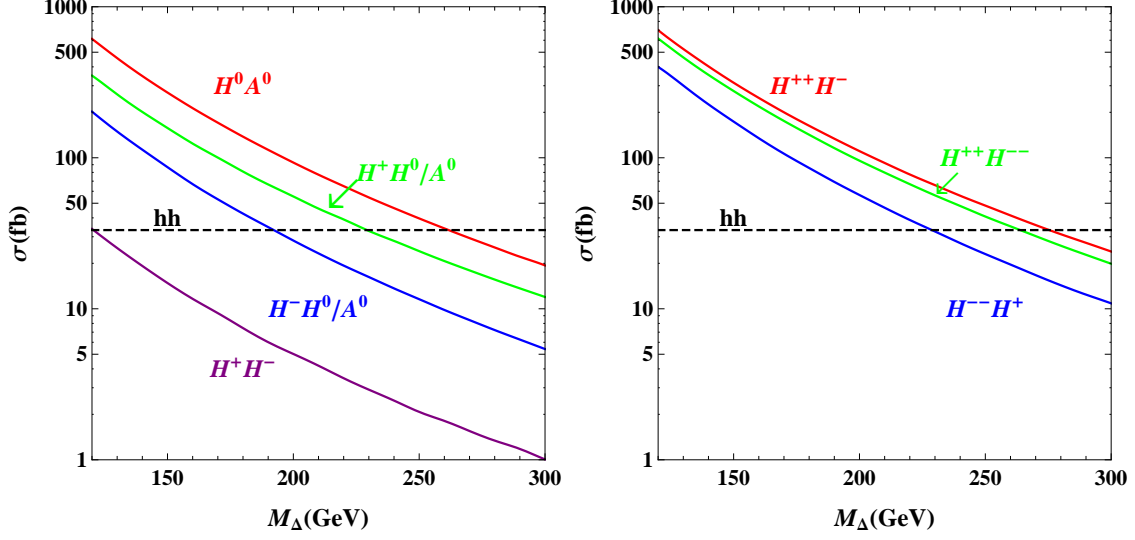


FIG. 9. Production cross sections for a pair of scalars at LHC14 versus M_Δ for a degenerate spectrum. The black dashed line is for the SM hh production.

For the same reason, in the negative scenario where H^0/A^0 are the lightest, the charged scalars contribute instead to the production of H^0/A^0 through the cascade decays like $H^\pm \rightarrow H^0/A^0 W^*$. In this work, we study these contributions in the same way as was done for the positive scenario in Refs. [67, 68].

We define the reference cross section X_0 for the standard Drell-Yan process

$$X_0 = \sigma(pp \rightarrow Z^* \rightarrow H^0 A^0), \quad (10)$$

which is independent of the cascade decay parameters v_Δ and ΔM . A detailed study on the $b\bar{b}\tau^+\tau^-$ signal for this process with $M_\Delta = 130$ GeV can be found in Ref. [1]. Besides the above direct production, neutral scalars can also be produced from cascade decays of charged scalars. These extra production channels include $H^\pm H^0/A^0$, $H^+ H^-$, $H^\pm H^\mp$, and $H^{++} H^{--}$ followed by cascade decays of charged scalars. We consider first the associated $H^\pm H^0/A^0$ production followed by cascade decays of H^\pm ,

$$\begin{aligned} pp \rightarrow W^* \rightarrow H^\pm H^0 &\rightarrow H^0 H^0 W^*, \quad pp \rightarrow W^* \rightarrow H^\pm H^0 \rightarrow A^0 H^0 W^*, \\ pp \rightarrow W^* \rightarrow H^\pm A^0 &\rightarrow H^0 A^0 W^*, \quad pp \rightarrow W^* \rightarrow H^\pm A^0 \rightarrow A^0 A^0 W^*, \end{aligned} \quad (11)$$

resulting in three final states classified by a pair of neutral scalars: $A^0 H^0$, $H^0 H^0$, and $A^0 A^0$. Noting that the last two originate only from cascade decays, any detection of such production channels would be a hint of charged scalars being involved. Using the fact that

$$\sigma(pp \rightarrow W^* \rightarrow H^\pm H^0) \simeq \sigma(pp \rightarrow W^* \rightarrow H^\pm A^0), \quad (12)$$

$$\text{BR}(H^\pm \rightarrow H^0 W^*) \simeq \text{BR}(H^\pm \rightarrow A^0 W^*), \quad (13)$$

as well as the narrow width approximation, we calculate the production cross sections for these three final states:

$$H^0 A^0 : X_1 = 2[\sigma(pp \rightarrow W^+ \rightarrow H^+ H^0) + \sigma(pp \rightarrow W^- \rightarrow H^- H^0)] \times \text{BR}(H^\pm \rightarrow A^0 W^*), \quad (14)$$

$$H^0 H^0 : Y_1 = [\sigma(pp \rightarrow W^+ \rightarrow H^+ H^0) + \sigma(pp \rightarrow W^- \rightarrow H^- H^0)] \times \text{BR}(H^\pm \rightarrow H^0 W^*), \quad (15)$$

$$A^0 A^0 : Z_1 = [\sigma(pp \rightarrow W^+ \rightarrow H^+ A^0) + \sigma(pp \rightarrow W^- \rightarrow H^- A^0)] \times \text{BR}(H^\pm \rightarrow A^0 W^*). \quad (16)$$

The factor 2 in X_1 accounts for the equal contribution from the process with H^0 and A^0 interchanged. The relations $X_1 = 2Y_1 = 2Z_1$ actually hold true for all of the four production channels, since for a given channel the same branching ratios (such as for $H^\pm \rightarrow H^0/A^0 W^*$) are involved,

$$X_i = 2Y_i = 2Z_i, \quad (i = 1, 2, 3, 4), \quad (17)$$

where X_i , Y_i , and Z_i refer to the cross sections for $H^0 A^0$, $H^0 H^0$, and $A^0 A^0$ production with the subscript $i = 1, 2, 3, 4$ denoting the production channels $H^\pm H^0/A^0$, $H^+ H^-$, $H^\pm H^\mp$, and $H^{++} H^{--}$, respectively.

The relations imply that we may concentrate on the cross section of $H^0 A^0$ production.

Naively, one would expect the next important channel to be $H^+ H^-$ since it only involves two cascade decays:

$$X_2 = 2\sigma(pp \rightarrow \gamma^*/Z^* \rightarrow H^+ H^-) \times \text{BR}(H^\pm \rightarrow H^0 W^*)\text{BR}(H^\pm \rightarrow A^0 W^*). \quad (18)$$

But as already mentioned in Ref. [68], a smaller coupling and destructive interference between the γ^* and Z^* exchange make the cross section of $H^+ H^-$ production an order of magnitude smaller than that of $H^0 A^0$ even for a degenerate spectrum. Considering further suppression due to cascade decays, X_2 is not important for the enhancement of $H^0 A^0$ production and can be safely neglected in the numerical analysis.

The contribution from $H^\pm H^\mp$ is more important despite the fact that it involves three cascade decays:

$$X_3 = 2[\sigma(pp \rightarrow W^{*-} \rightarrow H^+ H^{--}) + \sigma(pp \rightarrow W^{*+} \rightarrow H^- H^{++})] \times \text{BR}(H^{\pm\pm} \rightarrow H^\pm W^*)\text{BR}(H^\pm \rightarrow H^0 W^*)\text{BR}(H^\pm \rightarrow A^0 W^*). \quad (19)$$

As shown in Fig. 9, $\sigma(pp \rightarrow W^* \rightarrow H^\pm H^\mp)$ is the largest for a degenerate mass spectrum. When cascade decays are dominant, the phase-space suppression of heavy charged scalars will be important. So we expect that the $H^0 A^0$ production receives considerable enhancement from $H^\pm H^\mp$ when the mass splitting is small and cascade decays are dominant.

Finally, the last mechanism is $H^{++} H^{--}$, which involves four cascade decays:

$$X_4 = 2\sigma(pp \rightarrow \gamma^*/Z^* \rightarrow H^{++} H^{--}) \times \text{BR}(H^{\pm\pm} \rightarrow H^\pm W^*)^2 \times \text{BR}(H^\pm \rightarrow H^0 W^*)\text{BR}(H^\pm \rightarrow A^0 W^*). \quad (20)$$

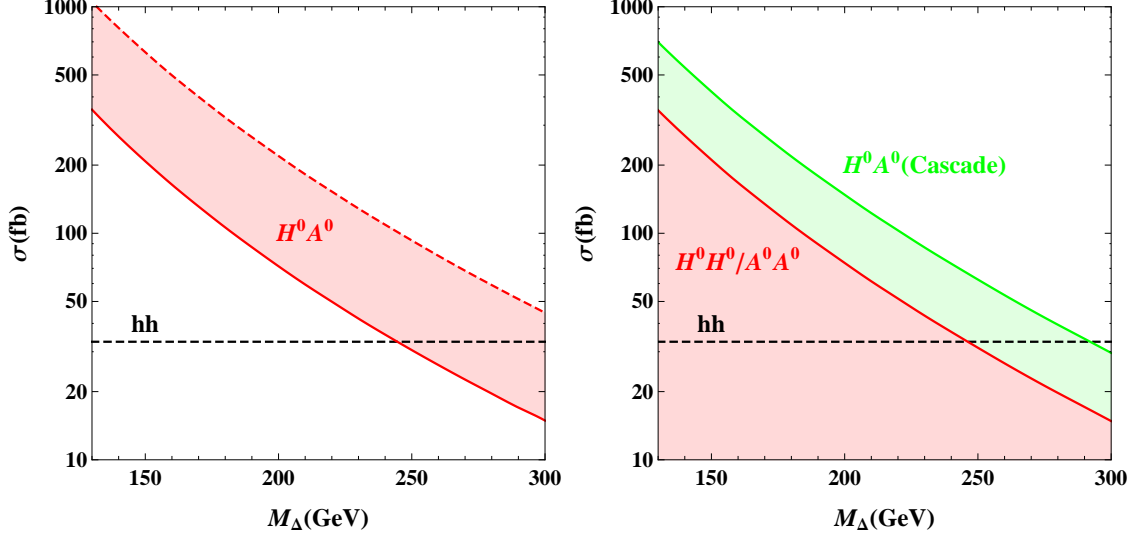


FIG. 10. Production cross sections for a pair of neutral scalars versus M_Δ at LHC14 and with $\Delta M = 5$ GeV, $v_\Delta = 0.001$ GeV. Left: The red solid (dashed) line corresponds to X_0 (X). Right: The red line corresponds to $H^0 H^0 / A^0 A^0$ from cascade decays Y/Z , and the green line to $H^0 A^0$ from cascade decays (X_C). The shaded regions are filled by scanning over ΔM and v_Δ .

This mechanism is also promising since the cross section of $H^{++}H^{--}$ production is slightly larger than $H^0 A^0$ production for a degenerate mass spectrum. The phase-space suppression of X_4 is more severe than that of X_3 , because a pair of the heaviest $H^{\pm\pm}$ are produced.

Summing over all four of the above channels yields the contribution to the $H^0 A^0$ production from cascade decays,

$$X_C = X_1 + X_2 + X_3 + X_4, \quad (21)$$

and the total production cross section of $H^0 A^0$ is then $X = X_0 + X_C$. Using Eq. (17), the total cross sections for the pair production $H^0 H^0 / A^0 A^0$, $Y = \sum_i Y_i$, $Z = \sum_i Z_i$, are given by

$$Y = Z = \frac{1}{2} X_C. \quad (22)$$

Since the enhancement from cascade decays depends on a not severely suppressed phase space and a larger branching ratio of cascade decays, we choose to work with a relatively smaller mass splitting and triplet vev as shown in Eq. (9). Figure 10 displays the cross sections of the $H^0 A^0$, $H^0 H^0$, and $A^0 A^0$ production as a function of M_Δ . As can be seen from the figure, the production of $H^0 A^0$ can be enhanced by a factor of 3, while the $H^0 H^0 / A^0 A^0$ production at the maximal enhancement can reach the level of X_0 . This could make the detection of neutral scalar pair productions very promising in the negative scenario.

IV. LHC SIGNATURES OF NEUTRAL SCALAR PRODUCTION

In this section we investigate the signatures of neutral scalar production at the LHC. From previous studies on the SM hh production, we already know that the most promising signal is $b\bar{b}\gamma\gamma$, and $b\bar{b}\tau^+\tau^-$ is next to it, while both semileptonic and dileptonic decays of W 's in the $b\bar{b}W^+W^-$ channel are challenging. In this work we analyze all three of the signals— $b\bar{b}\gamma\gamma$, $b\bar{b}\tau^+\tau^-$, and $b\bar{b}W^+W^- \rightarrow b\bar{b}\ell^+\ell^-2\nu$ ($\ell = e, \mu$ for collider identification)—as well as their backgrounds based on the benchmark model presented in Eq. (9).

In Sec. III we discussed the Drell-Yan production of $H^0 A^0$ and the enhanced pair and associated production of neutral scalars H^0/A^0 due to cascade decays of charged scalars H^\pm , $H^{\pm\pm}$. We are now ready to incorporate the branching ratios of H^0/A^0 decays for a specific signal channel. For instance, the cross sections for the $b\bar{b}\gamma\gamma$ signal channel can be written as

$$S_0(b\bar{b}\gamma\gamma) = X_0 \times [\text{BR}(H^0 \rightarrow b\bar{b})\text{BR}(A^0 \rightarrow \gamma\gamma) + \text{BR}(H^0 \rightarrow \gamma\gamma)\text{BR}(A^0 \rightarrow b\bar{b})], \quad (23)$$

$$S(b\bar{b}\gamma\gamma) = X \times [\text{BR}(H^0 \rightarrow b\bar{b})\text{BR}(A^0 \rightarrow \gamma\gamma) + \text{BR}(H^0 \rightarrow \gamma\gamma)\text{BR}(A^0 \rightarrow b\bar{b})] \\ + 2Y \times \text{BR}(H^0 \rightarrow b\bar{b})\text{BR}(H^0 \rightarrow \gamma\gamma) + 2Z \times \text{BR}(A^0 \rightarrow b\bar{b})\text{BR}(A^0 \rightarrow \gamma\gamma). \quad (24)$$

Here S_0 denotes the signal from the direct production $pp \rightarrow Z^* \rightarrow H^0 A^0$ alone, and S includes contributions from cascade decays. $S_{(0)}(b\bar{b}\tau^+\tau^-)$ has a similar expression as $S_{(0)}(b\bar{b}\gamma\gamma)$, while $S_{(0)}(b\bar{b}\ell^+\ell^-2\nu)$ is simpler since the decay mode $A^0 \rightarrow W^+W^-$ is absent.

The theoretical cross sections for the $b\bar{b}\gamma\gamma$, $b\bar{b}\tau^+\tau^-$, and $b\bar{b}\ell^+\ell^-2\nu$ signal channels are plotted in Fig. 11. The cross section $S_0(b\bar{b}\gamma\gamma)/S_0(b\bar{b}\tau^+\tau^-)$ is larger than that of the SM hh production until $M_\Delta = 159/161$ GeV; taking into account cascade enhancement pushes the corresponding M_Δ further to 179/197 GeV. $S_0(b\bar{b}\ell^+\ell^-2\nu)$ is always larger than that of hh in the mass region 130-200 GeV, and interestingly, it keeps about the same value when $M_\Delta < 160$ GeV. The signal from $H^0 H^0$ is comparable with S_0 in these three channels only for $M_\Delta < 160$ GeV, while in contrast the signal from $A^0 A^0$ becomes dominant for the $b\bar{b}\gamma\gamma$ and $b\bar{b}\tau^+\tau^-$ channels when $M_\Delta > 160$ GeV. Therefore, we have a chance to probe the $A^0 A^0$ pair production in these two channels. Also shown in Fig. 11 is the enhancement factor S/S_0 for the three signal channels at the benchmark point (9) as a function of M_Δ , which will help us understand the simulation results.

A. $b\bar{b}\gamma\gamma$ signal channel

In our simulation, the parton-level signal and background events are generated with **MADGRAPH5** [69]. We perform parton shower and fast detector simulations with **PYTHIA** [70] and **DELPHES3** [71]. Finally,

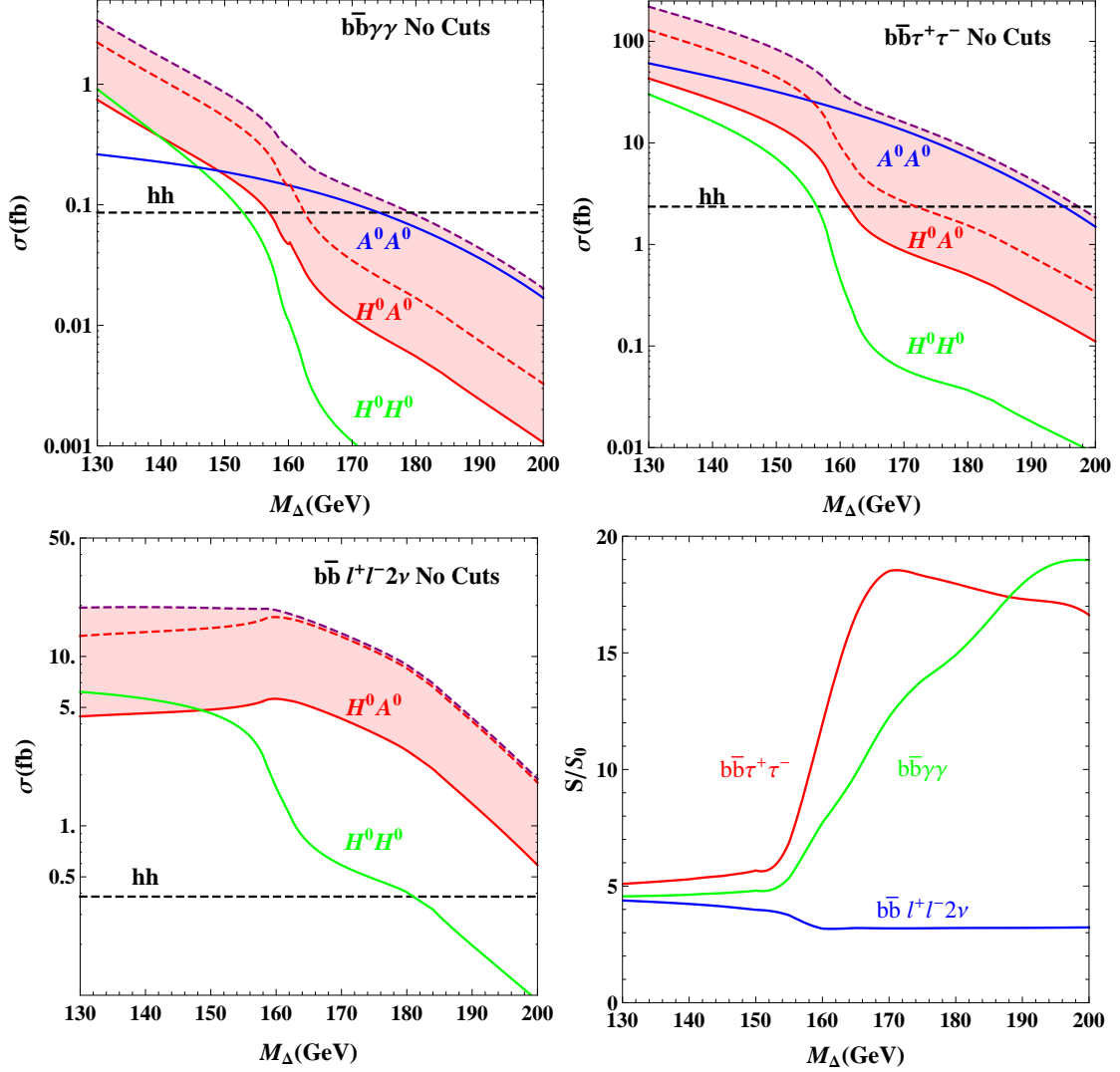


FIG. 11. Theoretical cross sections of $b\bar{b}\gamma\gamma$, $b\bar{b}\tau^+\tau^-$, and $b\bar{b}l^+l^-2\nu$ signal channels at LHC14. The red solid (dashed) line corresponds to the signal from X_0 (X), the green (blue) solid line corresponds to the signal from Y (Z), and the purple dashed line shows the total cross section S for the signal. The SM hh cross section is shown for comparison. The lower right panel shows the enhancement factor S/S_0 in the three signal channels.

MADANALYSIS5 [72] is responsible for data analysis and plotting. We take a flat b -tagging efficiency of 70%, and mistagging rates of 10% for c jets and 1% for light-flavor jets, respectively. Jet reconstruction is done using the anti- k_T algorithm with a radius parameter of $R = 0.5$. We further assume a photon identification efficiency of 85% and a jet-faking-photon rate of 1.2×10^{-4} [73].

The main SM backgrounds to the signal are as follows:

$$b\bar{b}\gamma\gamma : pp \rightarrow b\bar{b}\gamma\gamma, \quad (25)$$

$$t\bar{t}h : pp \rightarrow t\bar{t}h \rightarrow b\ell^+\nu \bar{b}\ell^-\nu \gamma\gamma (\ell^\pm \text{ missed}), \quad (26)$$

$$Zh : pp \rightarrow Zh \rightarrow b\bar{b}\gamma\gamma. \quad (27)$$

Among them, $b\bar{b}\gamma\gamma$ and Zh are irreducible, while $t\bar{t}h$ is reducible and can be reduced by vetoing the additional ℓ 's with $p_T^\ell > 20$ GeV and $|\eta_\ell| < 2.4$. In addition, there exist many reducible sources of fake $b\bar{b}\gamma\gamma$:

$$\begin{aligned} pp \rightarrow b\bar{b}jj &\rightarrow b\bar{b}\gamma\gamma, pp \rightarrow b\bar{b}j\gamma \rightarrow b\bar{b}\gamma\gamma, \dots \\ pp \rightarrow c\bar{c}\gamma\gamma &\rightarrow b\bar{b}\gamma\gamma, pp \rightarrow j\bar{j}\gamma\gamma \rightarrow b\bar{b}\gamma\gamma, \dots, \end{aligned} \quad (28)$$

where $x \rightarrow y$ stands for a final-state x misidentified as y . The remaining fake sources are subdominant and are thus not included in our simulation. The QCD corrections to the backgrounds are included by a multiplicative K -factor of 1.10 and 1.33 for the leading cross sections of $t\bar{t}h$ and Zh at LHC14 [74], respectively. The cross section of the $b\bar{b}\gamma\gamma$ background has been normalized to include fake sources and does not take NLO corrections into account.

The distributions of some kinematical variables before applying any cuts are shown in Fig. 12, where we assume $M_\Delta = 130, 160, 190$ GeV. In our analysis, we require that the final states include exactly one b -jet pair and one γ pair and satisfy the following basic cuts:

$$p_T^{b,\gamma} > 30 \text{ GeV}, |\eta_{b,\gamma}| < 2.4, \Delta R_{bb,\gamma\gamma} > 0.4, \quad (29)$$

where $\Delta R = \sqrt{(\Delta\phi)^2 + (\Delta\eta)^2}$ is the particle separation, with $\Delta\phi$ and $\Delta\eta$ being the separation in the azimuthal angle and rapidity, respectively. Here we employ a tighter p_T cut than is usually applied to suppress the QCD-electroweak $b\bar{b}\gamma\gamma$ background. The b -jet pair and γ pair are then required to fall in the following windows on the invariant masses and fulfill the ΔR cut criteria:

$$\Delta R_{bb} < 2.5, |M_{bb} - M_\Delta| < 15 \text{ GeV}, \quad (30)$$

$$\Delta R_{\gamma\gamma} < 2.5, |M_{\gamma\gamma} - M_\Delta| < 10 \text{ GeV}.$$

As shown in Fig. 12, the $\Delta R_{bb,\gamma\gamma}$ distributions of the signal are clearly more compact as they are more likely coming from the same particles. Thus the ΔR cuts can effectively suppress the background. More specific cuts are necessary for further analysis. A useful variable is the invariant mass of the neutral scalar pair $M_{H^0 A^0}$, and the total transverse energy E_T is also distinctive. The peak of $M_{H^0 A^0}$ increases with M_Δ , and similarly for E_T . For simplicity, we adopt for the cuts a linear shift between $M_{H^0 A^0}$, E_T and M_Δ :

$$M_{H^0 A^0} > 2M_\Delta + 90 \text{ GeV}, E_T > 2M_\Delta - 60 \text{ GeV}. \quad (31)$$

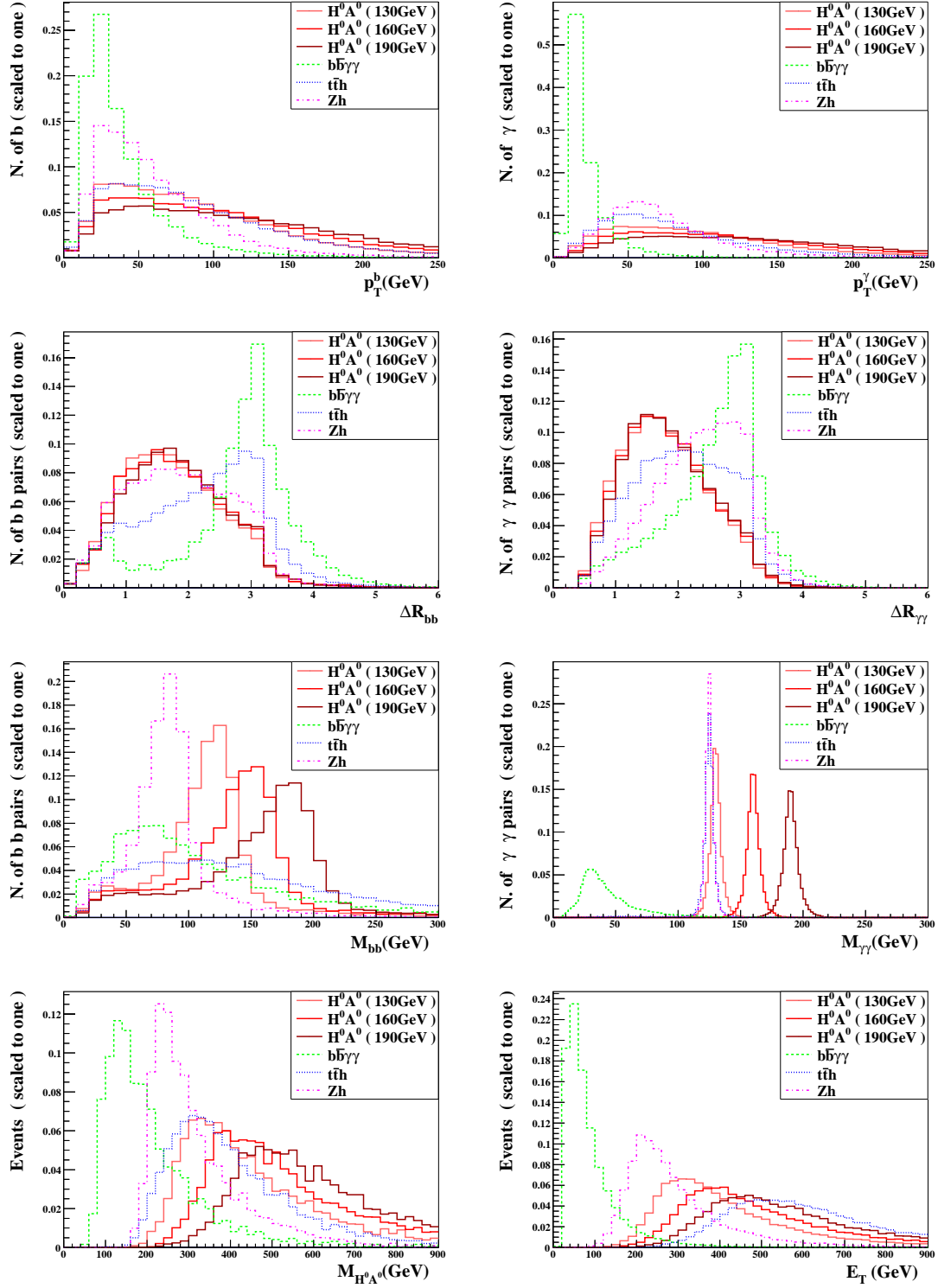


FIG. 12. Distributions of $p_T^{b,\gamma}$, $\Delta R_{bb,\gamma\gamma}$, $M_{bb,\gamma\gamma,H^0 A^0}$, and E_T for the signal $bb\gamma\gamma$ and its backgrounds before applying any cuts at LHC14.

$M_\Delta = 130 \text{ GeV}$	$H^0 A^0(S_0)$	$b\bar{b}\gamma\gamma$	$t\bar{t}h$	Zh	S/B	$\mathcal{S}(S, B)$
Cross section at NLO	8.01×10^{-1}	5.92×10^3	1.18	2.99×10^{-1}	1.39×10^{-4}	5.75×10^{-1}
Basic cuts	1.22×10^{-1}	4.16×10^1	1.03×10^{-1}	3.41×10^{-2}	2.92×10^{-3}	1.03
Reconstruct scalars from bs	6.99×10^{-2}	7.07	1.50×10^{-2}	9.61×10^{-4}	9.87×10^{-3}	1.44
Reconstruct scalars from γs	5.28×10^{-2}	1.03×10^{-1}	1.08×10^{-2}	7.32×10^{-4}	4.63×10^{-1}	8.01
Cut on $M_{H^0 A^0}$	4.21×10^{-2}	2.04×10^{-2}	4.69×10^{-3}	3.23×10^{-4}	1.65	12.0
Cut on E_T	3.31×10^{-2}	6.58×10^{-3}	4.68×10^{-3}	2.27×10^{-4}	2.88	12.8
Cascade enhanced	1.51×10^{-1}	—	—	—	13.1	41.0
$M_\Delta = 160 \text{ GeV}$	$H^0 A^0(S_0)$	$b\bar{b}\gamma\gamma$	$t\bar{t}h$	Zh	S/B	$\mathcal{S}(S, B)$
Cross section at NLO	5.10×10^{-2}	5.92×10^3	1.18	2.99×10^{-1}	8.61×10^{-6}	3.63×10^{-2}
Basic cuts	8.78×10^{-3}	4.16×10^1	1.03×10^{-1}	3.41×10^{-2}	2.10×10^{-4}	7.44×10^{-2}
Reconstruct scalars from bs	4.11×10^{-3}	5.06	1.34×10^{-2}	2.36×10^{-4}	8.11×10^{-4}	9.99×10^{-2}
Reconstruct scalars from γs	3.27×10^{-3}	3.42×10^{-2}	1.57×10^{-5}	0.00	9.56×10^{-2}	9.53×10^{-1}
Cut on $M_{H^0 A^0}$	2.57×10^{-3}	1.12×10^{-2}	1.18×10^{-5}	0.00	2.30×10^{-1}	1.28
Cut on E_T	1.73×10^{-3}	3.95×10^{-3}	1.03×10^{-5}	0.00	4.37×10^{-1}	1.41
Cascade enhanced	1.10×10^{-2}	—	—	—	2.77	7.29
$M_\Delta = 190 \text{ GeV}$	$H^0 A^0(S_0)$	$b\bar{b}\gamma\gamma$	$t\bar{t}h$	Zh	S/B	$\mathcal{S}(S, B)$
Cross section at NLO	2.68×10^{-3}	5.92×10^3	1.18	2.99×10^{-1}	4.53×10^{-7}	1.91×10^{-3}
Basic cuts	5.33×10^{-4}	4.16×10^1	1.03×10^{-1}	3.41×10^{-2}	1.28×10^{-5}	4.52×10^{-3}
Reconstruct scalars from bs	2.27×10^{-4}	3.61	1.05×10^{-2}	1.24×10^{-4}	6.27×10^{-5}	6.53×10^{-3}
Reconstruct scalars from γs	1.81×10^{-4}	2.47×10^{-2}	3.93×10^{-6}	0.00	7.34×10^{-3}	6.30×10^{-2}
Cut on $M_{H^0 A^0}$	1.55×10^{-4}	9.87×10^{-3}	3.93×10^{-6}	0.00	1.57×10^{-2}	8.52×10^{-2}
Cut on E_T	8.35×10^{-5}	1.48×10^{-3}	3.93×10^{-6}	0.00	5.63×10^{-2}	1.18×10^{-1}
Cascade enhanced	1.50×10^{-3}	—	—	—	1.01	1.87

TABLE I. Evolution of signal and background cross sections (in fb) at LHC14 for the $b\bar{b}\gamma\gamma$ signal channel upon imposing the cuts one by one. For the cascade-enhanced signal only the cross section passing all the cuts is shown. The last two columns assume an integrated luminosity of 3000 fb^{-1} .

For instance, we apply $M_{H^0 A^0} > 350 \text{ GeV}$, $E_T > 200 \text{ GeV}$ at the benchmark point $M_\Delta = 130 \text{ GeV}$.

To estimate the observability quantitatively, we adopt the following significance measurement:

$$\mathcal{S}(S, B) = \sqrt{2 \left((S \cdot \mathcal{L} + B \cdot \mathcal{L}) \log \left(1 + \frac{S}{B} \right) - S \cdot \mathcal{L} \right)}, \quad (32)$$

which is more suitable than the usual definition of S/\sqrt{B} or $S/\sqrt{S+B}$ for Monte Carlo analysis [75]. Here S and B are the signal and background cross sections, and \mathcal{L} is the integrated luminosity. The survival cross sections of the signal from the Drell-Yan process and of the backgrounds upon imposing cuts step by

step are summarized in Table I at the benchmark point (9) for $M_\Delta = 130, 160, 190$ GeV respectively. For the cascade-enhanced signal, only the cross section passing all the cuts is shown. The last two columns in the table show the signal-to-background ratio S/B and the statistical significance $\mathcal{S}(S, B)$.

For $M_\Delta = 130$ GeV, the $b\bar{b}\gamma\gamma$ channel is very promising. Without (with) cascade enhancement, the final significance can reach 12.8 (41) for LHC14@3000, corresponding to 99 (453) events. For $M_\Delta = 160$ GeV, the channel becomes challenging since the cross section has decreased by a factor of 15.7 compared with the case of $M_\Delta = 130$ GeV. But the cuts we applied are efficient to suppress the SM background, and with cascade enhancement the significance could still reach 7.29 for 3000 fb $^{-1}$, corresponding to 33 events in the most optimistic case. For $M_\Delta = 190$ GeV, it looks hopeless even with maximal cascade enhancement in our benchmark model: to achieve 10 signal events, an integrated luminosity of at least 6670 fb $^{-1}$ is required, which is beyond the reach of the future LHC.

B. $b\bar{b}\tau^+\tau^-$ signal channel

For this signal channel, an important part of the analysis depends on the ability to reconstruct the b pair and the τ pair. Here we consider the hadronic decays of the τ lepton and assume a τ -tagging efficiency of 70% with a negligible fake rate.

The main SM backgrounds are as follows:

$$b\bar{b}\tau^+\tau^- : pp \rightarrow b\bar{b}Z/\gamma^*/h \rightarrow b\bar{b}\tau^+\tau^-, \quad (33)$$

$$b\bar{b}W^+W^- : pp \rightarrow b\bar{b}W^+W^- \rightarrow b\bar{b}\tau^+\nu_\tau\tau^-\bar{\nu}_\tau, \quad (34)$$

$$Zh : pp \rightarrow Zh \rightarrow b\bar{b}\tau^+\tau^-. \quad (35)$$

The irreducible QCD-electroweak background comes from $b\bar{b}\tau^+\tau^-$, where the τ pair originates from the decays of $Z/\gamma^*/h$. Since the hadronic decays of τ always contain neutrinos, we also include the SM background $b\bar{b}W^+W^-$, which contributes to the $b\bar{b}\tau^+\nu_\tau\tau^-\bar{\nu}_\tau$ final state. The $b\bar{b}W^+W^-$ background mainly originates from $t\bar{t}$ production with subsequent decays $t \rightarrow bW$ and $W \rightarrow \tau\nu_\tau$. Moreover, the associated Zh production gets involved through the subsequent decays $h \rightarrow b\bar{b}$ and $Z \rightarrow \tau^+\tau^-$ or vice versa. The QCD corrections to the backgrounds are included by a multiplicative K -factor of 1.21, 1.35, and 1.33 to the leading cross section of $b\bar{b}\tau^+\tau^-$ [76], $t\bar{t}$ [77], and Zh [74] at LHC14.

The kinematical distributions similar to the $b\bar{b}\gamma\gamma$ channel are shown in Fig. 13. As one can see from the figure, the τ jets are less energetic than the b jets (similar to those in the $b\bar{b}\gamma\gamma$ signal channel) due to missing neutrinos in the final state. We first employ the following selection cuts to pick up signals with exactly one

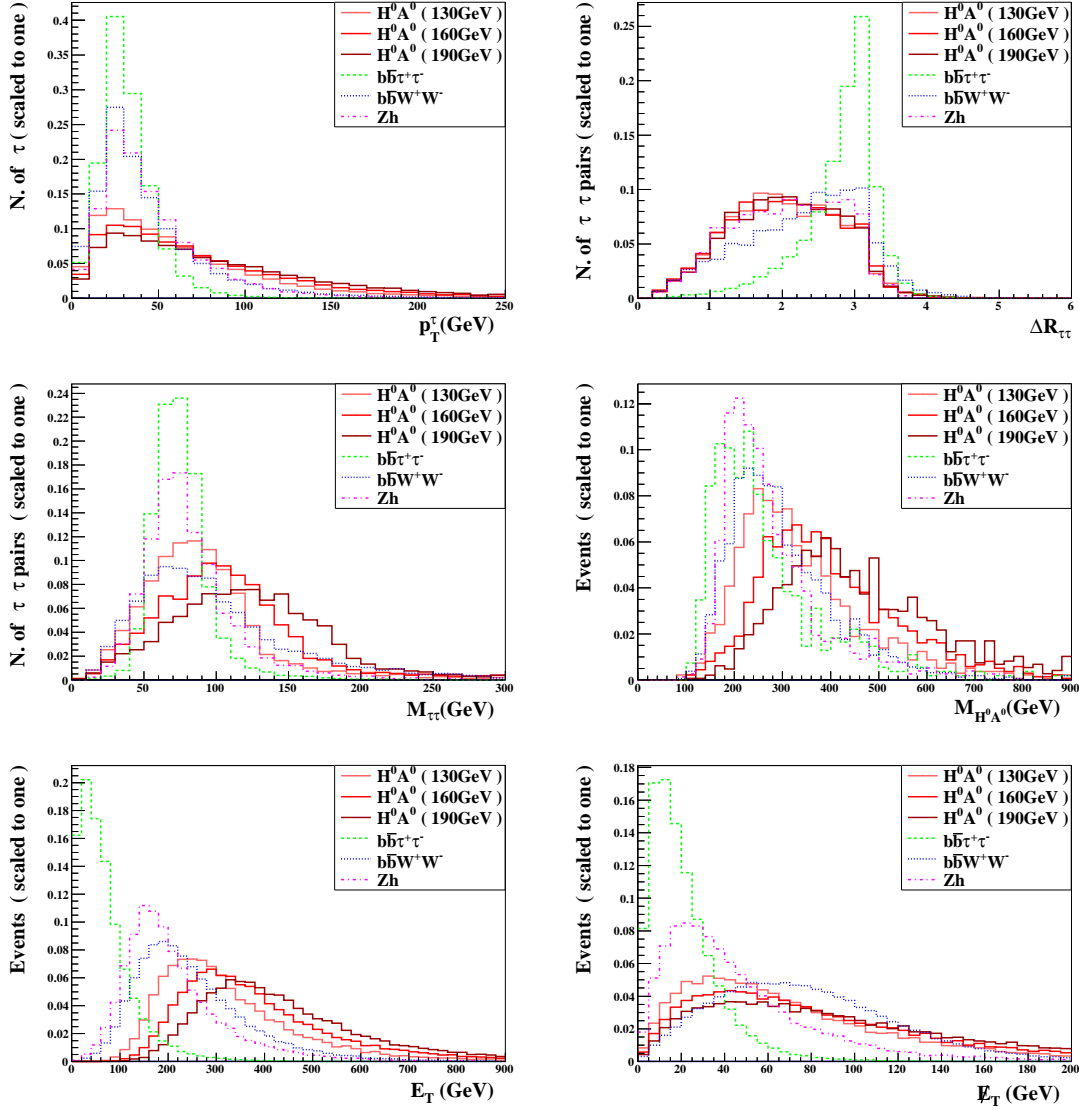


FIG. 13. Distributions of p_T^τ , $\Delta R_{\tau\tau}$, $M_{\tau\tau, H^0 A^0}$, E_T , and \cancel{E}_T for the signal $b\bar{b}\tau^+\tau^-$ and its backgrounds before applying any cuts at LHC14.

b pair and one τ pair:

$$p_T^{b,\tau} > 30 \text{ GeV}, |\eta_{b,\tau}| < 2.4, \Delta R_{bb,b\tau,\tau\tau} > 0.4, \quad (36)$$

and no cut on \cancel{E}_T is adopted. After the selection, the τ and b pairs are required to fulfill the cuts on the invariant masses and separations:

$$\Delta R_{\tau\tau} < 2.5, M_\Delta - 40 \text{ GeV} < M_{\tau\tau} < M_\Delta, \quad (37)$$

$$\Delta R_{bb} < 2.5, |M_{bb} - M_\Delta| < 15 \text{ GeV}.$$

$M_\Delta = 130 \text{ GeV}$	$H^0 A^0(S_0)$	$b\bar{b}\tau^+\tau^-$	$b\bar{b}W^+W^-$	Zh	S/B	$\mathcal{S}(S, B)$
Cross section at NLO	4.31×10^1	3.10×10^4	7.92×10^3	2.21×10^1	1.11×10^{-3}	12.0
Basic cuts	7.75×10^{-1}	4.49×10^1	8.97×10^1	2.91×10^{-1}	5.74×10^{-3}	3.65
Reconstruct scalars from τ s	5.14×10^{-1}	1.19×10^1	3.57×10^1	1.06×10^{-1}	1.08×10^{-2}	4.06
Reconstruct scalars from b s	2.14×10^{-1}	4.34	9.44×10^{-1}	2.28×10^{-2}	4.04×10^{-2}	5.06
Cut on $M_{H^0 A^0}$	1.29×10^{-1}	1.96×10^{-1}	1.51×10^{-1}	8.10×10^{-3}	3.64×10^{-1}	11.3
Cut on E_T	1.03×10^{-1}	9.87×10^{-2}	7.35×10^{-2}	5.89×10^{-3}	5.81×10^{-1}	12.4
Cascade enhanced	5.27×10^{-1}	—	—	—	2.96	51.6
$M_\Delta = 160 \text{ GeV}$	$H^0 A^0(S_0)$	$b\bar{b}\tau^+\tau^-$	$b\bar{b}W^+W^-$	Zh	S/B	$\mathcal{S}(S, B)$
Cross section at NLO	3.08	3.10×10^4	7.92×10^3	2.21×10^1	7.92×10^{-5}	8.55×10^{-1}
Basic cuts	6.81×10^{-2}	4.49×10^1	8.97×10^1	2.91×10^{-1}	5.05×10^{-4}	3.21×10^{-1}
Reconstruct scalars from τ s	3.14×10^{-2}	1.52×10^1	2.46×10^2	3.17×10^{-2}	1.20×10^{-3}	3.36×10^{-1}
Reconstruct scalars from b s	1.2×10^{-2}	2.47	1.06×10^{-1}	0.00	4.80×10^{-3}	4.10×10^{-1}
Cut on $M_{H^0 A^0}$	6.99×10^{-3}	1.22×10^{-1}	2.06×10^{-2}	0.00	4.89×10^{-2}	1.00
Cut on E_T	5.04×10^{-3}	4.72×10^{-2}	5.88×10^{-3}	0.00	9.48×10^{-2}	1.18
Cascade enhanced	5.11×10^{-2}	—	—	—	9.63×10^{-1}	10.7
$M_\Delta = 190 \text{ GeV}$	$H^0 A^0(S_0)$	$b\bar{b}\tau^+\tau^-$	$b\bar{b}W^+W^-$	Zh	S/B	$\mathcal{S}(S, B)$
Cross section at NLO	2.47×10^{-1}	3.10×10^4	7.92×10^3	2.21×10^1	6.34×10^{-6}	6.86×10^{-2}
Basic cuts	6.54×10^{-3}	4.49×10^1	8.97×10^1	2.91×10^{-1}	4.86×10^{-5}	3.09×10^{-2}
Reconstruct scalars from τ s	2.32×10^{-3}	4.60×10^{-1}	1.47×10^1	5.89×10^{-3}	1.53×10^{-4}	3.26×10^{-2}
Reconstruct scalars from b s	7.66×10^{-4}	2.06×10^{-2}	1.21	0.00	6.25×10^{-4}	3.78×10^{-2}
Cut on $M_{H^0 A^0}$	6.34×10^{-4}	1.47×10^{-3}	9.03×10^{-2}	0.00	6.91×10^{-3}	1.14×10^{-1}
Cut on E_T	3.87×10^{-4}	0.00	2.64×10^{-2}	0.00	1.47×10^{-2}	1.30×10^{-1}
Cascade enhanced	6.85×10^{-3}	—	—	—	2.60×10^{-1}	2.22

TABLE II. Similar to Table I, but for the $b\bar{b}\tau^+\tau^-$ signal channel.

The different mass shift between $M_{\tau\tau}$ and M_{bb} is owing to the missing neutrinos in τ decays resulting in a wider distribution of $M_{\tau\tau}$. For the reconstructed neutral scalars, we further adopt similar cuts on $M_{H^0 A^0}$ and E_T as in the $b\bar{b}\gamma\gamma$ channel:

$$M_{H^0 A^0} > 2M_\Delta + 70 \text{ GeV}, \quad E_T > 2M_\Delta - 80 \text{ GeV}. \quad (38)$$

Both $M_{H^0 A^0}$ and E_T cuts are reduced by 20 GeV compared with the $b\bar{b}\gamma\gamma$ channel, which again results from neutrinos in the final state. The corresponding results are summarized in Table II.

The $b\bar{b}\tau^+\tau^-$ is also promising for $M_\Delta = 130 \text{ GeV}$ even without enhancement from cascade decays. The final significance is 12.4 and the corresponding number of signal events is 309 for LHC14@3000.

Including the cascade enhancement, the significance is improved to 51.6, which is even better than the $b\bar{b}\gamma\gamma$ signal. For $M_\Delta = 160$ GeV, the biggest challenge is also the small production cross section of the signal. But in the most optimistic case, the cascade decays can increase the signal by a factor of 10.1, making this channel feasible. Finally, neutral scalars as heavy as 190 GeV are difficult to detect at LHC14 in this channel.

C. $b\bar{b}W^+W^-$ signal channel

It is difficult to search for the SM Higgs pair production in this channel due to missing energy brought about by neutrinos in leptonic decays of the W boson, which makes one of the two Higgs bosons not fully reconstructible [36, 57]. The situation is ameliorated in our scenario because, the production rate of $H^0 A^0$ can be an order of magnitude larger than that of hh and the di- W decay branching ratio of H^0 can also be larger than h in the vast parameter space. This considerably improves the signal events and partially compensates the deficiency of the detection capability.

With both W 's decaying leptonically, the final state appears as $b\bar{b}\ell^+\ell^-\cancel{E}_T$. The dominant SM backgrounds are as follows:

$$t\bar{t} : pp \rightarrow t\bar{t} \rightarrow bW^+\bar{b}W^- \rightarrow b\bar{b}\ell^+\ell^-\cancel{E}_T. \quad (39)$$

As before, the QCD correction is included by a multiplicative K -factor of 1.35 for the $t\bar{t}$ production [77]. We pick up the events that include exactly one b -jet pair and one opposite-sign lepton pair and filter them with the basic cuts:

$$p_T^b > 30 \text{ GeV}, p_T^\ell > 20 \text{ GeV}, |\eta_{b,\ell}| < 2.4, \quad (40)$$

$$\Delta R_{bb,b\ell,\ell\ell} > 0.4, \cancel{E}_T > 20 \text{ GeV}.$$

The separation and invariant mass of the b -jet pair are required to fulfill

$$\Delta R_{bb} < 2.5, |M_{bb} - M_\Delta| < 15 \text{ GeV}. \quad (41)$$

For the lepton pair, we reconstruct the transverse cluster mass $M_C^{\ell\ell}$:

$$M_C^{\ell\ell} = \sqrt{\left(\sqrt{p_{T,\ell\ell}^2 + M_{\ell\ell}^2} + \cancel{E}_T\right)^2 + \left(\vec{p}_{T,\ell\ell} + \vec{\cancel{E}}_T\right)^2}. \quad (42)$$

The distributions of $M_C^{\ell\ell}$, $\Delta R_{\ell\ell}$, and \cancel{E}_T are shown in Fig. 14. The peak of $M_C^{\ell\ell}$ is always lower than M_Δ by about 30-40 GeV, and the lepton separation $\Delta R_{\ell\ell}$ in the signal is much smaller than in the $t\bar{t}$ background. Accordingly, we set a wide window on $M_C^{\ell\ell}$ while tightening up the cuts on $\Delta R_{\ell\ell}$ and \cancel{E}_T :

$$M_\Delta - 80 \text{ GeV} < M_C^{\ell\ell} < M_\Delta, \Delta R_{\ell\ell} < 1.2, \cancel{E}_T > 0.9M_\Delta. \quad (43)$$

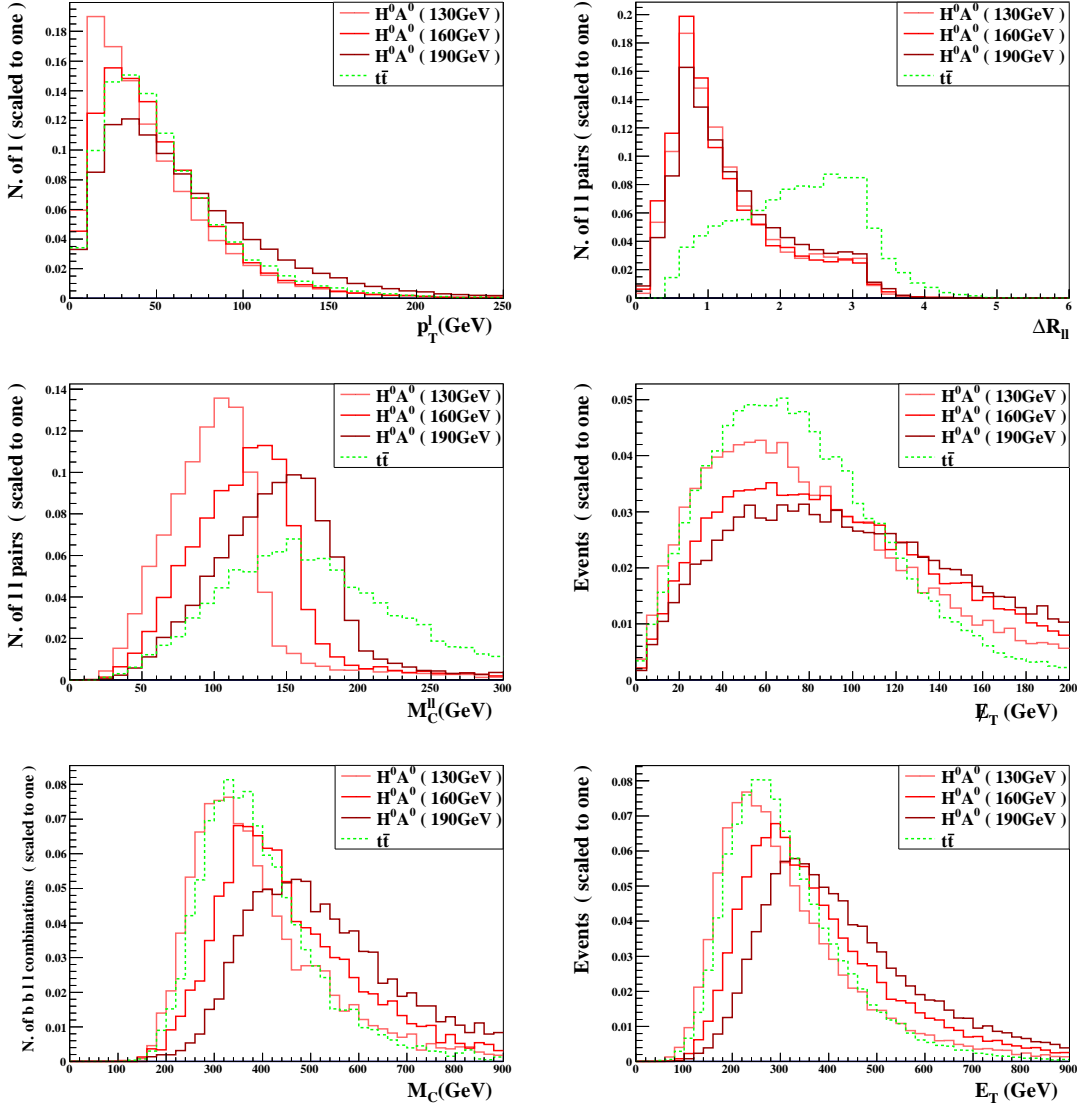


FIG. 14. Distributions of p_T^ℓ , $\Delta R_{\ell\ell}$, $M_C^{\ell\ell}$, \cancel{E}_T , M_C , and E_T for the signal $b\bar{b}\ell^+\ell^-\cancel{E}_T$ and its backgrounds before applying any cuts at LHC14.

We find that $M_C^{\ell\ell}$ is least efficient around $M_\Delta \sim 190$ GeV, where the peak of $M_C^{\ell\ell}$ for the $t\bar{t}$ background is around 150 GeV. The very tight cuts on $\Delta R_{\ell\ell}$ and \cancel{E}_T are sufficient to suppress the background by 1 or 2 orders of magnitude, while keeping the number of signal events as large as possible. We further combine the b -jet pair and the lepton pair into a cluster and construct the transverse cluster mass:

$$M_C = \sqrt{\left(\sqrt{p_{T,b\ell\ell}^2 + M_{b\ell\ell}^2} + \cancel{E}_T\right)^2 - \left(\vec{p}_{T,b\ell\ell} + \vec{\cancel{E}}_T\right)^2}, \quad (44)$$

which is an analog of $M_{H^0A^0}$ in the previous subsection. The distribution of M_C is displayed in Fig. 14, which is very similar to that of $M_{H^0A^0}$ in the $b\bar{b}\gamma\gamma$ channel. Although it looks from the M_C distributions

$M_\Delta = 130 \text{ GeV}$	$H^0 A^0(S_0)$	$t\bar{t}$	S/B	$\mathcal{S}(S, B)$
Cross section at NLO	3.91	2.38×10^4	1.69×10^{-4}	1.41
Basic cuts	1.51	4.04×10^3	3.74×10^{-4}	1.30
Reconstruct scalars from bs	3.29×10^{-1}	3.35×10^2	9.82×10^{-4}	0.984
Cut on $M_C^{\ell\ell}$	3.21×10^{-1}	2.14×10^2	1.50×10^{-3}	1.20
Cut on $\Delta R_{\ell\ell}$	2.64×10^{-1}	9.26×10^1	2.85×10^{-3}	1.50
Cut on \cancel{E}_T	8.45×10^{-2}	1.48×10^1	5.71×10^{-3}	1.20
Cut on M_C	3.30×10^{-2}	1.69×10^{-1}	1.95×10^{-1}	4.26
Cut on E_T	3.19×10^{-2}	1.47×10^{-1}	2.17×10^{-1}	4.41
Cascade enhanced	1.40×10^{-1}	—	9.53×10^{-1}	17.7
$M_\Delta = 160 \text{ GeV}$	$H^0 A^0(S_0)$	$t\bar{t}$	S/B	$\mathcal{S}(S, B)$
Cross section at NLO	4.95	2.38×10^4	2.13×10^{-4}	1.78
Basic cuts	2.13	4.04×10^3	5.27×10^{-4}	1.84
Reconstruct scalars from bs	4.25×10^{-1}	2.68×10^2	1.59×10^{-3}	1.42
Cut on $M_C^{\ell\ell}$	3.97×10^{-1}	1.89×10^2	2.10×10^{-3}	1.58
Cut on $\Delta R_{\ell\ell}$	3.21×10^{-1}	7.04×10^1	4.56×10^{-3}	2.09
Cut on \cancel{E}_T	9.47×10^{-2}	4.29	2.21×10^{-2}	2.50
Cut on M_C	3.28×10^{-2}	4.74×10^{-2}	6.92×10^{-1}	7.50
Cut on E_T	3.02×10^{-2}	3.62×10^{-2}	8.34×10^{-1}	7.78
Cascade enhanced	1.01×10^{-1}	—	3.24	23.2
$M_\Delta = 190 \text{ GeV}$	$H^0 A^0(S_0)$	$t\bar{t}$	S/B	$\mathcal{S}(S, B)$
Cross section at NLO	1.19	2.38×10^4	5.00×10^{-5}	0.424
Basic cuts	6.44×10^{-1}	4.04×10^3	1.59×10^{-4}	0.554
Reconstruct scalars from bs	1.36×10^{-1}	2.26×10^2	6.02×10^{-4}	0.495
Cut on $M_C^{\ell\ell}$	1.27×10^{-1}	1.79×10^2	7.09×10^{-4}	0.520
Cut on $\Delta R_{\ell\ell}$	9.70×10^{-2}	6.05×10^1	1.60×10^{-3}	0.683
Cut on \cancel{E}_T	2.57×10^{-2}	1.62	1.59×10^{-2}	1.10
Cut on M_C	8.85×10^{-3}	1.89×10^{-2}	4.68×10^{-1}	3.29
Cut on E_T	8.37×10^{-3}	1.40×10^{-2}	5.98×10^{-1}	3.56
Cascade enhanced	2.69×10^{-2}	—	1.92	10.1

TABLE III. Similar to Table I, but for the $b\bar{b}\ell^+\ell^-\cancel{E}_T$ signal channel.

(before any cuts are made) that the $t\bar{t}$ background has a large overlap with the signal, the cuts on $M_C^{\ell\ell}$, $\Delta R_{\ell\ell}$, and \cancel{E}_T actually modify them remarkably, so that a further cut on M_C could improve the significance

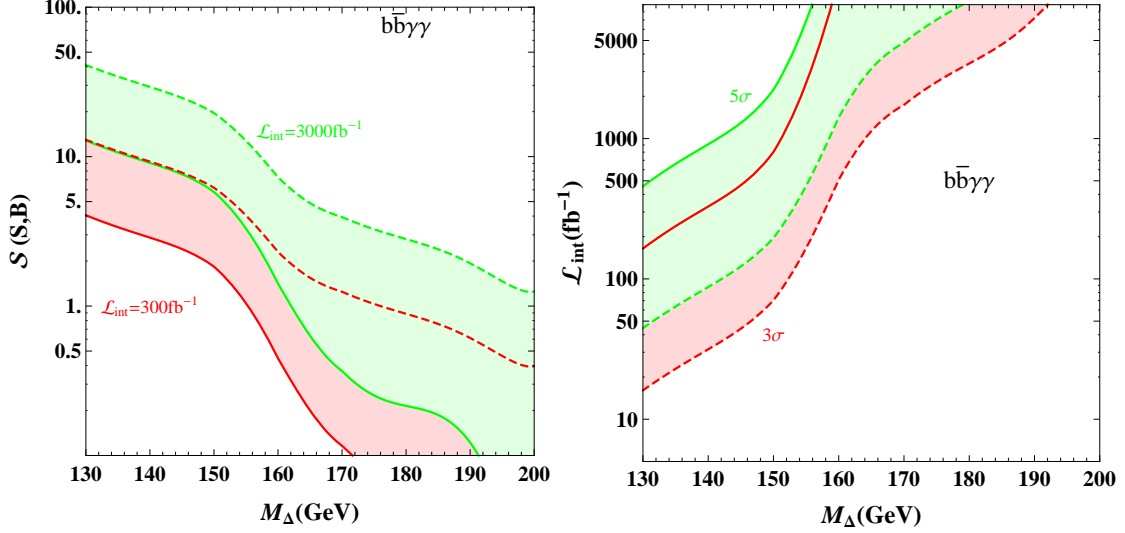


FIG. 15. Left: Significance $\mathcal{S}(S,B)$ of the $b\bar{b}\gamma\gamma$ channel versus M_Δ reachable at LHC14@300 (red region) and LHC14@3000 (green). Right: Required luminosity to reach a 3σ (red region) and 5σ (green) significance in the $b\bar{b}\gamma\gamma$ channel versus M_Δ at LHC14. The solid line corresponds to the signal from X_0 alone, and the dashed line corresponds to the total signal including cascade enhancement.

efficiently. We apply a cut on M_C as we did with $M_{H^0 A^0}$, as well as one on E_T :

$$M_C > 2M_\Delta + 90 \text{ GeV}, \quad E_T > 2M_\Delta - 60 \text{ GeV}. \quad (45)$$

The results following the cutflow are summarized in Table III. For $M_\Delta = 130$ GeV, the final significance is 4.41 (17.7) without (with) cascade enhancement. With cascade enhancement this should be enough to discover the neutral scalars. The signal channel is more promising for $M_\Delta = 160$ GeV due to a slightly larger cross section and higher cut efficiencies. The final significance is 7.78 (23.2), which is also better than the $b\bar{b}\gamma\gamma$ and $b\bar{b}\tau^+\tau^-$ channels with the same mass. Finally, for $M_\Delta = 190$ GeV, the significance becomes 3.56 (10.1). Therefore, for our benchmark model, the only promising signal for such heavy neutral scalars (~ 190 GeV) comes from the $b\bar{b}W^+W^-$ channel.

D. Observability

Based on our elaborate analysis of signal channels in Secs. IV A–IV C, we examine the observability of the neutral scalars H_0 , A_0 in the mass region $130 \sim 200$ GeV by adopting essentially the same cuts as before. In the left panel of Figs. 15, 16, and 17 we present the significance $\mathcal{S}(S,B)$ as a function of M_Δ in the three signal channels $b\bar{b}\gamma\gamma$, $b\bar{b}\tau^+\tau^-$, and $b\bar{b}\ell^+\ell^- \cancel{E}_T$ that is reachable for LHC14@300 and LHC14@3000, respectively. The required luminosity to achieve a 3σ and 5σ significance is displayed in

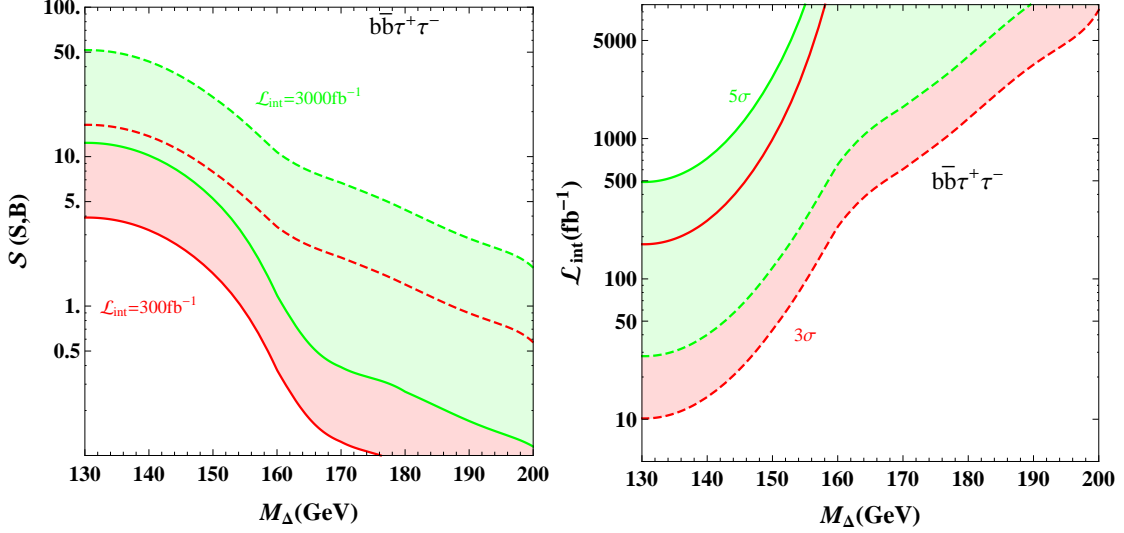


FIG. 16. Same as Fig. 15, but for the $b\bar{b}\tau^+\tau^-$ channel.

the right panel of the figures. As was done in our previous analysis, the effect of cascade enhancement is included by a factor S/S_0 in the final results.

As shown in Figs. 15 and 16, both the $b\bar{b}\gamma\gamma$ and $b\bar{b}\tau^+\tau^-$ channel are typically sensitive to the low-mass region ($M_\Delta \lesssim 160$ GeV). In the absence of cascade enhancement, the 3σ significance would never be reached for $M_\Delta \gtrsim 138$ (142) GeV in the $b\bar{b}\gamma\gamma$ ($b\bar{b}\tau^+\tau^-$) channel for LHC14@300. However, a cascade enhancement of $S/S_0 \sim 4 - 6$ (as can be seen from Fig. 11) in this mass region can greatly improve the observability, pushing the 3σ mass limit up to 157 (162) GeV in the $b\bar{b}\gamma\gamma$ ($b\bar{b}\tau^+\tau^-$) channel. Moreover, with cascade enhancement, one has a good chance to reach a 5σ significance if $M_\Delta \lesssim 153$ (155) GeV. In other words, the cascade enhancement significantly reduces the required luminosity. For instance, to achieve a 3σ and 5σ significance in the $b\bar{b}\gamma\gamma$ ($b\bar{b}\tau^+\tau^-$) channel with $M_\Delta = 130$ GeV, the required luminosity is as low as 16 (10) fb^{-1} and 42 (27) fb^{-1} at LHC14, respectively. The $b\bar{b}\tau^+\tau^-$ channel is more promising, thanks to a relatively larger production rate.

At the future LHC14 with 3000 fb^{-1} data, the heavier mass region can also be probed. With a maximal cascade enhancement, the 3σ and 5σ mass reach is pushed to 177 and 164 GeV, respectively, in the $b\bar{b}\gamma\gamma$ channel, which should be compared to 156 and 151 GeV in the absence of enhancement. For the $b\bar{b}\tau^+\tau^-$ channel, the enhancement factor S/S_0 can reach about 18 above the W -pair threshold, upshifting the 3σ and 5σ mass reach to 189 and 177 GeV, respectively, from 154 and 150 GeV without the enhancement.

The $b\bar{b}\ell^+\ell^-\cancel{E}_T$ channel shown in Fig. 17 is more special, compared with $b\bar{b}\gamma\gamma$ and $b\bar{b}\tau^+\tau^-$. It is relatively more sensitive to a higher mass between 150-180 GeV, where the decay mode $H^0 \rightarrow W^+W^-$ dominates, while its observability deteriorates for $M_\Delta < 150$ GeV due to phase-space suppression in the

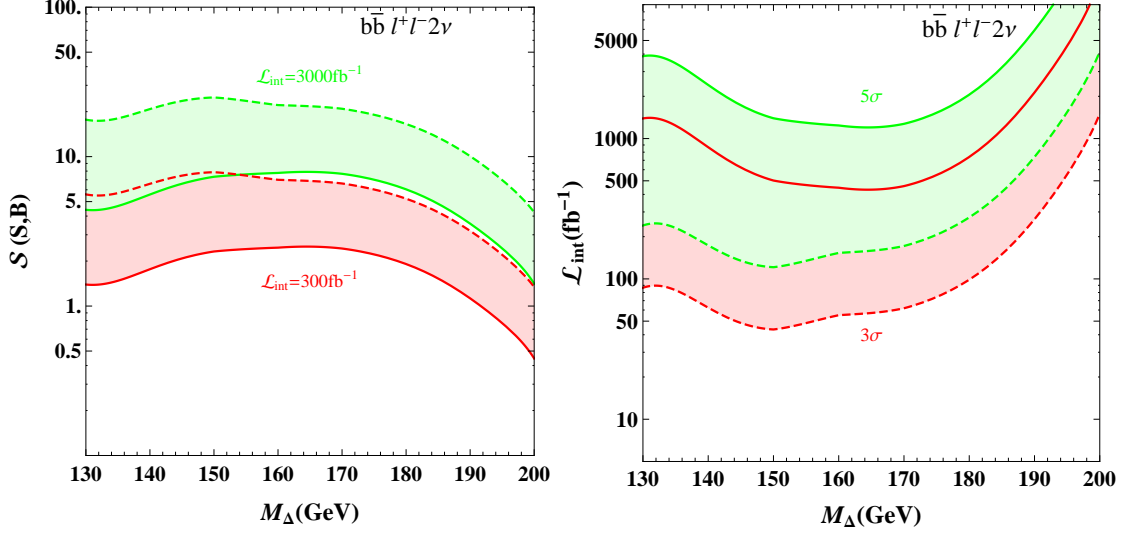


FIG. 17. Same as Fig. 15, but for the $b\bar{b}l^+l^-2\nu$ channel.

decay. The cascade enhancement S/S_0 at our benchmark point (9) is typically 3-4 in the mass region 130-200 GeV, and decreases as M_Δ increases. For LHC14@300, the 3σ and 5σ mass reach is, respectively, 190 and 181 GeV with maximal cascade enhancement. These limits would just increase by 2-3 GeV for LHC14@3000 if there were no cascade enhancement, while with cascade enhancement the 5σ limit, for instance, is pushed up to 200 GeV. Finally, a 3σ or 5σ reach in the mass region 150-180 GeV requires an integrated luminosity of 50 fb^{-1} (450 fb^{-1}) or 150 fb^{-1} (1300 fb^{-1}) with (without) cascade enhancement.

V. DISCUSSIONS AND CONCLUSIONS

In this paper, we have systematically investigated the LHC phenomenology of neutral scalar pair production in the negative scenario of the type II seesaw model. To achieve this goal, we first examined the decay properties of the neutral scalars H_0/A_0 and found that the scalar self-couplings λ_i have a great impact on the branching ratios of H^0/A^0 . The coupling λ_4 is important for tree-level decays of H^0 and A^0 , while one-loop-induced decays of H^0 further depend on λ_2 and λ_3 . We found that the decay $H^0 \rightarrow W^+W^-$ could dominate for $2M_W < M_{H^0} < 2M_h$ with $\lambda_4 < 0$, while it can be neglected once M_{H^0} is above the light scalar pair threshold $2M_h$. Moreover, the branching ratios of the decays $H^0 \rightarrow \gamma\gamma$, $Z\gamma$ can cross 3 orders of magnitude when varying the couplings λ_i , and there exist zero points for the H^0ZZ , H^0hh , and A^0Zh couplings.

The cross section of the Drell-Yan process $pp \rightarrow Z^* \rightarrow H^0A^0$ for $M_\Delta < 200$ GeV is much larger than that of the SM Higgs pair production driven by gluon fusion. In this paper, we studied the contributions

to H^0/A^0 production from cascade decays of the charged scalars H^\pm and $H^{\pm\pm}$. There are actually three different states for the neutral scalar pair: H^0A^0 , H^0H^0 , and A^0A^0 . Here, H^0H^0 and A^0A^0 can only arise from cascade decays of charged scalars, and their production rates always stay the same to a good approximation. Further, for a fixed value of M_Δ , cascade enhancement is determined by the variables v_Δ and ΔM . By tuning these two variables, the associated production rate of H^0A^0 can be maximally enhanced by about a factor of 3, while those of the H^0H^0 and A^0A^0 pair production can reach the value of H^0A^0 production through the pure Drell-Yan process.

We implemented detailed collider simulations of the associated H^0A^0 production for three typical signal channels ($b\bar{b}\gamma\gamma$, $b\bar{b}\tau^+\tau^-$, and $b\bar{b}W^+W^-$ with both W 's decaying leptonically). The enhancement from cascade decays of charged scalars is quantified by a multiplicative factor S/S_0 . Due mainly to a larger production rate, all three channels are more promising than the SM Higgs pair case. If there were no cascade enhancement, the 5σ mass reach of the $b\bar{b}\gamma\gamma$, $b\bar{b}\tau^+\tau^-$, and $b\bar{b}\ell^+\ell^-\cancel{E}_T$ channels would be, respectively, 151, 150, and 180 GeV for LHC14@3000. The cascade enhancement pushes these limits up to 164, 177, and 200 GeV. The $b\bar{b}\gamma\gamma$ and $b\bar{b}\tau^+\tau^-$ channels are more promising in the mass region below about 150 GeV, and the required luminosities for 5σ significance are 42 fb^{-1} and 27 fb^{-1} , respectively, at our benchmark point. Compared with these two channels, the $b\bar{b}\ell^+\ell^-\cancel{E}_T$ channel is more advantageous in the relatively higher mass region 150-200 GeV, and the required luminosity for 5σ significance is about 150 fb^{-1} with maximal cascade enhancement. Needless to say, for the purpose of a full investigation on the impact of heavy neutral scalars on the SM Higgs pair production, more sophisticated simulations are necessary. We hope that this work may shed some light on further studies in both the phenomenological and experimental communities.

ACKNOWLEDGMENTS

This work was supported in part by the Grants No. NSFC-11025525, No. NSFC-11575089 and by the CAS Center for Excellence in Particle Physics (CCEPP).

-
- [1] Z. L. Han, R. Ding, and Y. Liao, Phys. Rev. D **91**, 093006 (2015) [arXiv:1502.05242 [hep-ph]].
 - [2] G. Aad *et al.* [ATLAS Collaboration], Phys. Lett. B **726**, 88 (2013); Phys. Lett. B **734**, 406 (2014) [arXiv:1307.1427 [hep-ex]].
 - [3] S. Chatrchyan *et al.* [CMS Collaboration], JHEP **1306**, 081 (2013) [arXiv:1303.4571 [hep-ex]].
 - [4] G. Aad *et al.* [ATLAS Collaboration], Phys. Lett. B **716**, 1 (2012) [arXiv:1207.7214 [hep-ex]].

- [5] S. Chatrchyan *et al.* [CMS Collaboration], Phys. Lett. B **716**, 30 (2012) [arXiv:1207.7235 [hep-ex]].
- [6] T. Plehn, M. Spira, and P. M. Zerwas, Nucl. Phys. B **479**, 46 (1996) [Erratum-ibid. B **531**, 655 (1998)] [hep-ph/9603205].
- [7] S. Dawson, S. Dittmaier, and M. Spira, Phys. Rev. D **58**, 115012 (1998) [hep-ph/9805244].
- [8] A. Djouadi, W. Kilian, M. Muhlleitner, and P. M. Zerwas, Eur. Phys. J. C **10**, 45 (1999) [hep-ph/9904287].
- [9] U. Baur, T. Plehn, and D. L. Rainwater, Phys. Rev. D **67**, 033003 (2003) [hep-ph/0211224].
- [10] E. Asakawa, D. Harada, S. Kanemura, Y. Okada, and K. Tsumura, Phys. Rev. D **82**, 115002 (2010) [arXiv:1009.4670 [hep-ph]].
- [11] M. J. Dolan, C. Englert, and M. Spannowsky, JHEP **1210**, 112 (2012) [arXiv:1206.5001 [hep-ph]].
- [12] A. Papaefstathiou, L. L. Yang, and J. Zurita, Phys. Rev. D **87**, no. 1, 011301 (2013) [arXiv:1209.1489 [hep-ph]].
- [13] F. Goertz, A. Papaefstathiou, L. L. Yang, and J. Zurita, JHEP **1306**, 016 (2013) [arXiv:1301.3492 [hep-ph]].
- [14] R. S. Gupta, H. Rzehak, and J. D. Wells, Phys. Rev. D **88**, 055024 (2013) [arXiv:1305.6397 [hep-ph]].
- [15] A. J. Barr, M. J. Dolan, C. Englert, and M. Spannowsky, Phys. Lett. B **728**, 308 (2014) [arXiv:1309.6318 [hep-ph]].
- [16] D. de Florian and J. Mazzitelli, Phys. Rev. Lett. **111**, 201801 (2013) [arXiv:1309.6594 [hep-ph]].
- [17] M. J. Dolan, C. Englert, N. Greiner, and M. Spannowsky, Phys. Rev. Lett. **112**, 101802 (2014) [arXiv:1310.1084 [hep-ph]].
- [18] V. Barger, L. L. Everett, C. B. Jackson, and G. Shaughnessy, Phys. Lett. B **728**, 433 (2014) [arXiv:1311.2931 [hep-ph]].
- [19] C. Englert, F. Krauss, M. Spannowsky, and J. Thompson, Phys. Lett. B **743**, 93 (2015) [arXiv:1409.8074 [hep-ph]].
- [20] T. Liu and H. Zhang, arXiv:1410.1855 [hep-ph].
- [21] D. E. Ferreira de Lima, A. Papaefstathiou, and M. Spannowsky, JHEP **1408**, 030 (2014) [arXiv:1404.7139 [hep-ph]].
- [22] A. J. Barr, M. J. Dolan, C. Englert, D. E. F. de Lima, and M. Spannowsky, arXiv:1412.7154 [hep-ph].
- [23] M. J. Dolan, C. Englert, and M. Spannowsky, Phys. Rev. D **87**, no. 5, 055002 (2013) [arXiv:1210.8166 [hep-ph]].
- [24] A. Arhrib, R. Benbrik, C. -H. Chen, R. Guedes, and R. Santos, JHEP **0908**, 035 (2009) [arXiv:0906.0387 [hep-ph]].
- [25] N. Craig, J. Galloway, and S. Thomas, arXiv:1305.2424 [hep-ph].
- [26] B. Hespel, D. Lopez-Val, and E. Vryonidou, JHEP **1409**, 124 (2014) [arXiv:1407.0281 [hep-ph]].
- [27] G. D. Kribs and A. Martin, Phys. Rev. D **86**, 095023 (2012) [arXiv:1207.4496 [hep-ph]].
- [28] J. Cao, Z. Heng, L. Shang, P. Wan, and J. M. Yang, JHEP **1304**, 134 (2013) [arXiv:1301.6437 [hep-ph]].
- [29] D. T. Nhung, M. Muhlleitner, J. Streicher, and K. Walz, JHEP **1311**, 181 (2013) [arXiv:1306.3926 [hep-ph]].
- [30] U. Ellwanger, JHEP **1308**, 077 (2013) [arXiv:1306.5541 [hep-ph]].
- [31] B. Bhattacharjee and A. Choudhury, Phys. Rev. D **91**, 073015 (2015) [arXiv:1407.6866 [hep-ph]].
- [32] N. D. Christensen, T. Han, and T. Li, Phys. Rev. D **86**, 074003 (2012) [arXiv:1206.5816 [hep-ph]].
- [33] L. Wu, J. M. Yang, C. P. Yuan, and M. Zhang, Phys. Lett. B **747**, 378 (2015) [arXiv:1504.06932 [hep-ph]].

- [34] J. Cao, D. Li, L. Shang, P. Wu, and Y. Zhang, JHEP **1412**, 026 (2014) [arXiv:1409.8431 [hep-ph]].
- [35] C. Han, X. Ji, L. Wu, P. Wu, and J. M. Yang, JHEP **1404**, 003 (2014) [arXiv:1307.3790 [hep-ph]].
- [36] M. Gouzevitch, A. Oliveira, J. Rojo, R. Rosenfeld, G. P. Salam, and V. Sanz, JHEP **1307**, 148 (2013) [arXiv:1303.6636 [hep-ph]].
- [37] J. M. No and M. Ramsey-Musolf, Phys. Rev. D **89**, 095031 (2014) [arXiv:1310.6035 [hep-ph]].
- [38] R. Grober and M. Muhlleitner, JHEP **1106**, 020 (2011) [arXiv:1012.1562 [hep-ph]].
- [39] M. Gillioz, R. Grober, C. Grojean, M. Muhlleitner, and E. Salvioni, JHEP **1210**, 004 (2012) [arXiv:1206.7120 [hep-ph]].
- [40] J. Liu, X. P. Wang, and S. h. Zhu, arXiv:1310.3634 [hep-ph].
- [41] A. Arhrib, R. Benbrik, R. B. Guedes, and R. Santos, Phys. Rev. D **78**, 075002 (2008) [arXiv:0805.1603 [hep-ph]].
- [42] Z. Heng, L. Shang, Y. Zhang, and J. Zhu, JHEP **1402**, 083 (2014) [arXiv:1312.4260 [hep-ph]].
- [43] S. Dawson, E. Furlan, and I. Lewis, Phys. Rev. D **87**, 014007 (2013) [arXiv:1210.6663 [hep-ph]].
- [44] C. Y. Chen, S. Dawson, and I. M. Lewis, Phys. Rev. D **90**, 035016 (2014) [arXiv:1406.3349 [hep-ph]].
- [45] C. O. Dib, R. Rosenfeld, and A. Zerwekh, JHEP **0605**, 074 (2006) [hep-ph/0509179].
- [46] B. Yang, Z. Liu, N. Liu, and J. Han, Eur. Phys. J. C **74**, 3203 (2014) [arXiv:1408.4295 [hep-ph]].
- [47] C. Y. Chen, S. Dawson, and I. M. Lewis, Phys. Rev. D **91**, 035015 (2015) [arXiv:1410.5488 [hep-ph]].
- [48] R. Contino, M. Ghezzi, M. Moretti, G. Panico, F. Piccinini, and A. Wulzer, JHEP **1208**, 154 (2012) [arXiv:1205.5444 [hep-ph]].
- [49] K. Nishiwaki, S. Niyogi, and A. Shivaji, JHEP **1404**, 011 (2014) [arXiv:1309.6907 [hep-ph]].
- [50] N. Liu, S. Hu, B. Yang, and J. Han, JHEP **1501**, 008 (2015) [arXiv:1408.4191 [hep-ph]].
- [51] S. Dawson, A. Ismail, and I. Low, Phys. Rev. D **91**, 115008 (2015) [arXiv:1504.05596 [hep-ph]].
- [52] A. Azatov, R. Contino, G. Panico, and M. Son, Phys. Rev. D **92**, 035001 (2015) [arXiv:1502.00539 [hep-ph]].
- [53] F. Goertz, A. Papaefstathiou, L. L. Yang, and J. Zurita, JHEP **1504**, 167 (2015) [arXiv:1410.3471 [hep-ph]].
- [54] A. Pierce, J. Thaler, and L. -T. Wang, JHEP **0705**, 070 (2007) [hep-ph/0609049].
- [55] Z. Kang, P. Ko, and J. Li, arXiv:1504.04128 [hep-ph].
- [56] H. J. He, J. Ren, and W. Yao, arXiv:1506.03302 [hep-ph].
- [57] J. Baglio, A. Djouadi, R. Gröber, M. M. Mühlleitner, J. Quevillon, and M. Spira, JHEP **1304**, 151 (2013) [arXiv:1212.5581 [hep-ph]].
- [58] S. Dawson *et al.*, arXiv:1310.8361 [hep-ex].
- [59] T. P. Cheng and L. F. Li, Phys. Rev. D **22**, 2860 (1980); J. Schechter and J. W. F. Valle, Phys. Rev. D **22**, 2227 (1980); G. Lazarides, Q. Shafi, and C. Wetterich, Nucl. Phys. B **181**, 287 (1981); R. N. Mohapatra and G. Senjanovic, Phys. Rev. D **23**, 165 (1981); M. Magg and C. Wetterich, Phys. Lett. B **94**, 61 (1980).
- [60] A. Arhrib *et al.*, Phys. Rev. D **84**, 095005 (2011) [arXiv:1105.1925 [hep-ph]].
- [61] M. Aoki, S. Kanemura, M. Kikuchi, and K. Yagyu, Phys. Rev. D **87**, 015012 (2013) [arXiv:1211.6029 [hep-ph]]; S. Kanemura and K. Yagyu, Phys. Rev. D **85**, 115009 (2012) [arXiv:1201.6287 [hep-ph]].
- [62] M. Aoki, S. Kanemura, and K. Yagyu, Phys. Rev. D **85**, 055007 (2012) [arXiv:1110.4625 [hep-ph]].

- [63] M. Chabab, M. C. Peyranere, and L. Rahili, Phys. Rev. D **90**, 035026 (2014) [arXiv:1407.1797 [hep-ph]].
- [64] A. Djouadi, Phys. Rep. **459**, 1 (2008) [hep-ph/0503173].
- [65] P. Fileviez Perez, T. Han, G. -y. Huang, T. Li, and K. Wang, Phys. Rev. D **78**, 015018 (2008) [arXiv:0805.3536 [hep-ph]].
- [66] A. Melfo, M. Nemevsek, F. Nesti, G. Senjanovic, and Y. Zhang, Phys. Rev. D **85**, 055018 (2012) [arXiv:1108.4416 [hep-ph]].
- [67] E. J. Chun and P. Sharma, Phys. Lett. B **728**, 256 (2014) [arXiv:1309.6888 [hep-ph]].
- [68] A. G. Akeroyd and H. Sugiyama, Phys. Rev. D **84**, 035010 (2011) [arXiv:1105.2209 [hep-ph]].
- [69] J. Alwall, M. Herquet, F. Maltoni, O. Mattelaer, and T. Stelzer, JHEP **1106**, 128 (2011) [arXiv:1106.0522 [hep-ph]]; J. Alwall *et al.*, JHEP **1407**, 079 (2014) [arXiv:1405.0301 [hep-ph]].
- [70] T. Sjostrand, S. Mrenna, and P. Z. Skands, JHEP **0605**, 026 (2006) [hep-ph/0603175].
- [71] S. Ovin, X. Rouby, and V. Lemaître, arXiv:0903.2225 [hep-ph]; J. de Favereau *et al.* [DELPHES 3 Collaboration], JHEP **1402**, 057 (2014) [arXiv:1307.6346 [hep-ex]].
- [72] E. Conte, B. Fuks, and G. Serret, Comput. Phys. Commun. **184**, 222 (2013) [arXiv:1206.1599 [hep-ph]].
- [73] G. Aad *et al.* [ATLAS Collaboration], arXiv:0901.0512 [hep-ex].
- [74] S. Dittmaier *et al.* [LHC Higgs Cross Section Working Group Collaboration], arXiv:1101.0593 [hep-ph].
- [75] G. Cowan, K. Cranmer, E. Gross, and O. Vitells, Eur. Phys. J. C **71**, 1554 (2011) [Erratum-ibid. C **73**, 2501 (2013)] [arXiv:1007.1727 [physics.data-an]].
- [76] J. M. Campbell and R. K. Ellis, Phys. Rev. D **62**, 114012 (2000) [hep-ph/0006304].
- [77] M. Cacciari, S. Frixione, M. L. Mangano, P. Nason, and G. Ridolfi, JHEP **0809**, 127 (2008) [arXiv:0804.2800 [hep-ph]]; P. Bärnreuther, M. Czakon, and A. Mitov, Phys. Rev. Lett. **109**, 132001 (2012) [arXiv:1204.5201 [hep-ph]].